

# Multiscale Computational Approaches toward the Understanding of Materials

Marta Bordonhos, Tiago L. P. Galvão, José R. B. Gomes,\* José D. Gouveia, Miguel Jorge, Mirtha A. O. Lourenço, José M. Pereira, Germán Pérez-Sánchez, Moisés L. Pinto, Carlos M. Silva, João Tedim, and Bruno Zêzere

Herewith, an overview of the group's collaborative research efforts on the development and deployment of computational approaches to understand materials and tools at different length and time scales is presented. The techniques employed range from quantum mechanical approaches based on the density functional theory to classical atomistic and coarse-grained force field methods, targeting molecular systems composed of a few to several million atoms at different levels of detail. These new tools and molecular models are presented to the computational materials science community so they can be used in more realistic molecular modelling studies of the properties of materials and their dependence on subtle modifications of their structures. The review concludes by presenting a selection of recent computational case-studies oriented toward the understanding of the synthesis of materials, the interpretation of unexpected experimental results, the prediction of material properties, and the materials selection based on their characteristics for applications in areas such as gas adsorption/separation, corrosion protection, and catalysis.


for particular applications.<sup>[1]</sup> This is expected to yield tremendous benefits in areas such as catalysis, separation processes, carbon capture, and pollution control, where different families of materials are already widely employed. For example, the North American market for inorganic nanoporous and microporous materials for gas adsorption and separation processes is set to rise to 2.9 billion US dollars by the end of 2023 at a compound annual growth rate of 3.4% for the period of 2018–2023.<sup>[2]</sup> There are several different families of materials that have been attracting researchers' attention, particularly over the last 3 decades, from 1D (one-dimensional, e.g., carbon nanotubes), 2D (two-dimensional, e.g., graphene), to 3D (three-dimensional, e.g., zeolites) materials. Despite their great potential, further developments in tailored materials are limited by our lack of fundamental understanding and control over their synthesis processes, with most discoveries arising from the application of exhaustive searches or trial-and-error approaches.<sup>[3]</sup> It is clearly necessary to change this paradigm to enable the targeted design of new materials with tuned properties for a specific application, and computational methods are ideally suited for this purpose.

## 1. Introduction

For several decades, synthetic chemists, material scientists, and chemical engineers have pursued the goal of synthesizing materials by design to tailor their structural and interfacial properties

M. Bordonhos, J. R. B. Gomes, J. D. Gouveia, M. A. O. Lourenço, J. M. Pereira, G. Pérez-Sánchez, C. M. Silva, B. Zêzere  
CICECO - Aveiro Institute of Materials  
Department of Chemistry  
University of Aveiro  
Campus Universitário de Santiago  
Aveiro 3810-193, Portugal  
E-mail: jrgomes@ua.pt

M. Bordonhos, M. L. Pinto  
CERENA, Department of Chemical Engineering  
Instituto Superior Técnico  
University of Lisbon  
Avenida Rovisco Pais, No. 1, Lisbon 1049-001, Portugal  
T. L. P. Galvão, J. Tedim  
CICECO - Aveiro Institute of Materials  
Department of Materials and Ceramic Engineering  
University of Aveiro  
Campus Universitário de Santiago  
Aveiro 3810-193, Portugal  
M. Jorge  
Department of Chemical and Process Engineering  
University of Strathclyde  
75 Montrose Street, Glasgow G1 1XJ, UK

 The ORCID identification number(s) for the author(s) of this article can be found under <https://doi.org/10.1002/adts.202200628>

© 2022 The Authors. Advanced Theory and Simulations published by Wiley-VCH GmbH. This is an open access article under the terms of the Creative Commons Attribution-NonCommercial-NoDerivs License, which permits use and distribution in any medium, provided the original work is properly cited, the use is non-commercial and no modifications or adaptations are made.

DOI: 10.1002/adts.202200628

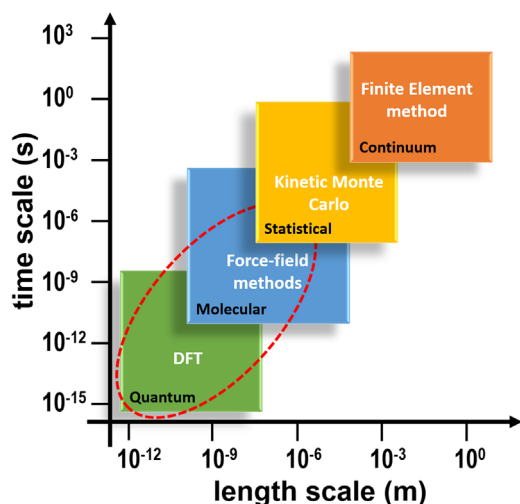


**Figure 1.** Families of computational materials science methods and corresponding time and length scales. The dashed red line highlights the density functional theory (DFT) and force field methods used and the scales reached in the studies that are reviewed in this work.

The exponential growth in computing power and the development of new theories and improved algorithms over the last 30 years has been making it possible to perform computer simulations with realistic models that provide in-depth understanding of the electronic and molecular structure of materials, which is of utmost importance in the characterization and prediction of their properties. In fact, while the first computational studies aimed to approximate the experimental findings used as benchmarks for model calibration, they were later used to confirm and aid in the interpretation of experimental observations and, more recently, they are being deployed to predict and anticipate properties under different operating conditions, including those of quite complex, hence more realistic, systems.<sup>[4–9]</sup> In parallel, databases with (calculated) data for an increasing number of materials are being created,<sup>[10,11]</sup> which is enabling the consideration of artificial intelligence and machine learning algorithms for screening the potential of existing and hypothetical materials for numerous applications.<sup>[12,13]</sup> Thus, we reached the point where well-calibrated computational studies can compete with experiments.

In this review article, we seek to provide an account of widely used computer simulation methods that are being used in computational materials science studies by providing an overview of some of our recent work focusing on the application of porous materials for gas adsorption and separation, corrosion protection, and heterogeneous catalysis. The computational approaches and the time/length scales that have been reached by the simulations reviewed in this work are shown in **Figure 1**.

The field of computational materials science is quite vast. Several computational strategies are not covered here (e.g., the kinetic Monte Carlo or the finite element method, Figure 1) for the sake of space and the reader interested in obtaining a more profound knowledge of the computer simulation approaches is directed to excellent books available in the literature.<sup>[14–16]</sup> Some simple application examples running on free highly-parallelized codes are provided for those aiming to initiate with the techniques of computational materials science.<sup>[15]</sup>

## 2. Computational Approaches

### 2.1. Density Functional Theory

Physicochemical phenomena at the electronic level are governed by the laws of quantum mechanics (QM), of which the Schrödinger equation is a key result. Computational methods that deal with phenomena at the electronic level are therefore based on solving this equation in some approximate way. The trust of the scientific community in computational methods in quantum chemistry has been immensely enhanced at least since 1998, when the Nobel Prize in Chemistry was awarded to Walter Kohn and John Pople for the development of density-functional theory (DFT) and of computational methods in quantum chemistry, respectively.<sup>[17]</sup> DFT is used to investigate the electronic properties of atoms, molecules, or solids, and is based on the two Hohenberg-Kohn (HK) theorems.<sup>[18]</sup> These two theorems are exact and, in short, establish that all the ground-state properties of a many-electron system can be determined if we know the spatial electronic density of the system. Every property of a quantum system can therefore be reduced to a functional of the electronic density. To find the electronic density as a function of the three spatial coordinates, one would in principle have to solve the Schrödinger equation of the system, which translates into solving a many-body problem of interacting electrons, an impractical (and often impossible) task. Kohn and Sham further built on the HK theorems and arrived at the Kohn-Sham (KS) equations,<sup>[19]</sup> which allow us to convert the problem of many interacting electrons into another one of noninteracting electrons in an effective potential, whose electronic density is the same as the original one.

Although the fundamentals of DFT are exact, the fact is that no formally exact exchange-correlation functional is known and approximations were constructed from first principles to satisfy properties of the exact functional (e.g., the local density approximation, LDA, and the generalized gradient approximation, GGA, among others that move the “Hartree World” closer to the “Heaven of Chemical Accuracy”<sup>[20]</sup>). Shortcomings of the DFT approaches in the lowest rungs of the Jacob’s ladder of density functional approximations for the exchange-correlation energy<sup>[20]</sup> will be, in principle, solved when using a more complicated approach from upper rungs of the ladder. However, it is not guaranteed that more complicated functionals always lead to improvements in the answers obtained with a less complicated functional, hence, the selection of a functional for a specific task is not trivial. Also, functionals from upper rungs of the Jacob’s ladder are computationally very expensive and, in practice, most contemporary DFT studies employ GGA approaches (from the second rung of the Jacob’s ladder) with an additional correction scheme to account for the long-range electron correlation (London dispersion interaction).<sup>[21,22]</sup> Additional approximations, for example, the Born–Oppenheimer approximation or the frozen core approximation are also important to make the calculations feasible.

The Born–Oppenheimer approximation consists of assuming that atomic nuclei are fixed in space and generate a static external potential, which is a consequence of the much larger relative mass of a nucleus compared to that of an electron. This means that the electronic wave function (and density) can be calculated

assuming stationary nuclei, but it does not mean that DFT cannot predict the ground state position of atoms. In fact, having determined the electronic density, one can calculate the forces acting upon nuclei. With this knowledge, one can estimate in which direction each atom should move to reach its ground-state position, and predict, for instance, molecule conformations or stable adsorption configurations.

The frozen core approximation replaces the electrons considered chemically inactive by an effective potential, the pseudopotential. Within this approximation, one typically considers that only the valence electrons (usually considered the most relevant for chemical reactions) are correlated and treated explicitly as waves, while the remaining electrons define the frozen core. This has the advantage of making the number of electrons to be treated explicitly considerably more manageable, and enables the inclusion of other effects, such as relativity. DFT codes often include their own pseudopotentials, which consist of large sets of numbers that define the behavior of atoms of each element.

The exact differential equations involved in DFT calculations can be turned into algebraic equations, more efficiently implemented computationally. This is done by representing the wave functions as linear combinations of basic functions. Often, periodic models use plane wave bases, while non-periodic ones use Gaussian-type orbitals.

DFT calculations are usually very computationally intensive due to the matrix operations involved. The calculation time taken by most DFT codes scales with the cubic power of the number of electrons, and the bottleneck is the diagonalization of the matrix corresponding to the KS equations. This means that codes with different diagonalization algorithms (such as sparse matrix algebra), or which avoid diagonalization completely, can scale differently with system size. Ref. [23] provides a comprehensive overview of some of these methods.

The explicit treatment of individual electrons allows one to calculate properties such as ground-state atomic bond distances and angles, bond and reaction energies, adsorption energies, vibrational frequencies and optical properties, reaction energy barriers, charge distributions and polarization, and many others. However, the fact that these methods have electronic detail severely limits the number of atoms that can be simulated in a reasonable amount of time to a few hundreds. For this reason, the simulation of processes that would require a very large number of molecules, for example, reactions occurring in a solution, employ certain tricks to simulate the solution environment. Examples include implicit solvation and microsolvation. Implicit solvation consists of assuming that the explicitly treated atoms are inserted in a continuous fluid, which acts as a dielectric field and thus adds a correction term to the calculations, while microsolvation is the inclusion of a few molecules of the fluid surrounding the reagents being studied, along with the assumption that the few fluid molecules are enough to cause the atoms of interest to behave as if they were immersed in a large volume of solvent. Since DFT can be used to calculate forces acting upon atoms, one can use it to simulate the dynamics of a quantum system given the initial positions and velocities of the species, by numerically integrating Newton's equations of motion. This is called *ab initio* molecular dynamics. Alternatively, physicochemical properties of systems calculated using first-principles methods can instead be fed into other kinds of models which do not treat electrons explic-

itly, allowing for the simulation of larger systems, as described below.

## 2.2. Classical Molecular Dynamics Simulations

Compared to DFT and other QM methods, molecular mechanics (MM) methods and classical molecular dynamics (MD) simulations neglect electronic degrees of freedom and treat molecules as a collection of atoms (or, more generally, interaction sites). MM methods have been widely employed to optimize the structures of large molecular systems or to provide an adequate embedding of the inner QM region in QM/MM calculations, while MD methods have been used to understand the dynamic evolution with time of complex systems with many degrees of freedom. They describe interatomic interactions by means of a force field and, in the case of MD methods, they also integrate the Newton's equations of motion to provide the position and speed of each species over time. The Hamiltonian is divided into non-bonded and bonded interactions, where the former includes an empirical potential function, commonly Lennard-Jones or Buckingham potentials, to describe the repulsion/dispersion forces between all pairs of atoms, together with a Coulomb term, which tackles the electrostatic interactions between charged moieties. The bonded terms describe the interactions between bonded atoms which comprise the molecule. The most common bonded functions for bond stretching, angle bending, and improper dihedrals are harmonic, while the periodicity of the potential associated with proper dihedrals is often represented by functions based on cosine series. Thus, selecting an adequate force field, encompassing the non-bonded and bonded parameters, is the cornerstone of any MD study and depends on the level of detail required for the analysis. At this point it is worth mentioning that polarizable force fields can effectively respond to subtle changes in the surrounding electric field. However, the computational burden for the possible higher accuracy may increase up to 10 times when compared with non-polarizable force fields, which are still the most used in classical MD simulations. Generally, the force field can involve a fully all-atom (AA) description, a united atom (UA) model without explicit hydrogens, where, for example CH, CH<sub>2</sub>, or CH<sub>3</sub> groups are treated as a single unified center with masses of  $\approx 13$ , 14, and 15 a. u., respectively, or a coarse-grained (CG) approach, where several atoms with similar physico-chemical characteristics are joined together into a larger interaction center, or "bead." The AA and UA levels are limited in size and time scale since they are very computationally demanding due to the number of interactions to consider, but still provide an adequate level of understanding at the nanoscopic scale. Generally, AA-MD and UA-MD simulations are restricted to thousands of atoms and hundreds of nanoseconds of simulation time, leaving out of the game processes such as long-range ordering or phase transitions. However, CG-MD models were developed to overcome AA-MD and UA-MD limitations by allowing the study of systems composed of millions of molecules and simulation times in the order of tens of microseconds. Additionally, the time step in CG simulations can be set to one order of magnitude higher than AA and UA approaches, thus the CG approach speeds up the dynamics by several orders of magnitude. This opens the door to fully addressing the synthesis of many soft materials, which requires a

minimum size/length to reproduce the self-assembly and formation of ordered phases.

The first CG simulation was performed four decades ago by Levitt et al.<sup>[24]</sup> reproducing the entire protein folding process. Since then, many CG approaches were developed from topology-based Gō models<sup>[25]</sup> to lattice Monte Carlo (MC) simulations tackling relatively large systems such as polymers<sup>[26]</sup> or nanoparticles.<sup>[27]</sup> Lattice MC studies also addressed the self-assembly of amphiphilic compounds<sup>[28–32]</sup> and zeolite formation.<sup>[33]</sup> However, two decades ago, the advent of the CG-MD MARTINI<sup>[34]</sup> (<http://cgmartini.nl>) force field brought fresh air into the CG computational community, becoming one of most popular CG approaches due to its reliability, simplicity, and transferability.<sup>[35]</sup> This model was developed based on experimental partitioning free energies of a wide number of chemical compounds.<sup>[35–40]</sup> MARTINI includes four pre-defined bead types for non-bonded interactions: Q, P, N, and C for charged, polar, non-polar, and apolar moieties, respectively. Five levels of polar or apolar strength (from 1 to 5) were considered in P and C bead types whereas acceptor(a), donor (d), donor-acceptor (da), or no (0) hydrogen bond capabilities were implicitly included as sublevels in N and Q bead types. The non-bonded parameters are summarized in the MARTINI matrix of interaction energies, making the parameter choice simpler. Additionally, “S” labelled beads symbolize a 3:1 mapping of heavy atoms to beads, specifically developed to mimic small organic rings upon reduction of the size and interaction energy of each bead. This allows the close packing of small ring moieties more closely without freezing, reproducing experimental data whilst preserving the correct partitioning behavior. Initially, MARTINI was designed for simulating lipids and some biomolecules,<sup>[34,41]</sup> but it was quickly extended to a wide number of organic and inorganic compounds of relevance in many areas.<sup>[38,40,42]</sup> Recently, a new, extended version of MARTINI, labelled MARTINI 3,<sup>[43]</sup> was launched, significantly improving the accuracy and breadth of application of this force field.

One of the main drawbacks of the classical approximation is that chemical reactions, which involve transfer of electrons between reacting atoms, cannot be explicitly described. Therefore, including chemical reactions in classical computer simulations is far from straightforward and requires specific “reactive” force fields or bespoke models. The first attempts were carried out in the 1970s by Moebis<sup>[44]</sup> and Gillespie<sup>[45]</sup> by means of MC simulations, later extended to reproduce real time-dependent reaction rate constants.<sup>[46]</sup> Since then, a lot of work has been done using MC,<sup>[47]</sup> kinetic Monte Carlo (KMC),<sup>[48]</sup> and MD simulations,<sup>[49]</sup> for example using specific force fields such as ReaxFF.<sup>[50,51]</sup> However, most of those studies make use of rather complicated models and/or algorithms, and are therefore limited to rather small system sizes, which poses problems when attempting to simultaneously describe mesoscale processes like self-assembly. Furthermore, standard reactive force fields require the use of very high temperatures or special sampling techniques in order to progress the reaction on a feasible time scale.<sup>[52]</sup> One option that has been pursued, mostly in simulations of polymer reactions, is to dynamically change bond topologies on-the-fly during an MD simulation.<sup>[53–57]</sup> However, this requires the development of specific scripts to stop the simulation, check for suitable chemical reactions, update the topology accordingly and restart the simula-

tion, which significantly slows down the simulations and hinders transferability.

One of the few studies to describe chemical reactions and self-assembly in material design was that of Lin et al.,<sup>[58]</sup> who developed an MC lattice model to simulate surfactant self-assembly and silica oligomerization at the same time, observing the formation of hexagonal and lamellar structures resembling the structures of mesoporous silica materials, albeit within the assumptions of their rather simplified model. Very recently, Carvalho et al.<sup>[59]</sup> successfully developed a CG MARTINI-based framework able to simultaneously describe chemical reactions and surfactant self-assembly using large systems in a computationally efficient way. The key to this approach was to describe the reaction using short-range continuous potentials that could be incorporated into highly-parallelized MD simulations. Despite the model being developed specifically for polymerization of silica in aqueous solutions with cetyl trimethyl ammonium bromide (CTAB) surfactants, the approach is general enough to be extended to other systems in which chemical reactions and self-assembly must be addressed together. Note that previous works attempting the CG-MD simulation of bond formation and bond breakage events in polymerization reactions considered the distance between pairs of particles evaluated at every N simulation time steps to decide ad-hoc which particles are bonded or non-bonded.<sup>[60]</sup>

### 2.3. Grand Canonical Monte Carlo

Like classical MD, the grand canonical Monte Carlo (GCMC) approach<sup>[61]</sup> relies on statistical mechanics under the classical approximation. This technique is used to simulate the properties of a system at thermodynamic equilibrium under constant temperature, chemical potential and volume, thus enabling fluctuations in both the energy and number of molecules of the system. In addition to the regular displacement movements used in standard canonical MC (molecule translations and rotations), trial insertions and deletions of molecules are attempted for allowing the number of particles to vary. All the random trial moves are handled by the normal Metropolis scheme<sup>[62]</sup> and are accepted or rejected according to criteria based on a Boltzmann-type weighting of the energy. Note that, unlike MD, MC approaches like GCMC do not rely on the dynamical method of time integration, hence high energy barriers and rare events can be circumvented through careful selection of the trial moves. The associated drawback is that the method does not follow the realistic dynamics of the system, and hence can only yield information about equilibrium properties.

Because the number of molecules in the simulation box is allowed to change, the GCMC approach is ideally suited to calculate the adsorption isotherms of gases by porous solid adsorbents, in contrast with MC simulations based on other ensembles. This is because we can directly calculate the average loading in the simulation cell at equilibrium under constant temperature and varying chemical potential, which can then be related to the pressure of the bulk gas in equilibrium with the adsorbed phase (most often through a thermodynamic equation of state). As such, a GCMC simulation is able to replicate experimental

measurements of adsorption isotherms, yielding the amount adsorbed as a function of bulk gas pressure. A particular advantage of GCMC for this purpose is that it can easily be extended to mixtures of any number of components. The computational procedure is the same as for pure components, except that identity change moves, where one molecule chosen randomly is switched to another component type in the mixture, are often introduced to increase computational efficiency (although they are not strictly required). It is common practice in GCMC simulations of adsorption to consider the structure of the adsorbent material as rigid, and hence the interactions between the gas and the solid are dictated by non-bonded interactions, that is, repulsion/dispersion forces and, when the adsorbates are polar molecules, also electrostatic interactions. The assumption of a rigid adsorbent structure will lead to inaccurate predictions of gas adsorption in materials with framework flexibility, like metal organic frameworks (MOFs) with breathing behavior. Noticeably, recent work showed that proper consideration of framework flexibility may be also important for simulation of the adsorption of aromatics in traditionally rigid materials like MFI-type zeolites.<sup>[63]</sup> Also, some MOFs may have unsaturated metal centers, the so-called open metal sites or coordinatively unsaturated sites, which can coordinate chemically to adsorbates like unsaturated hydrocarbons or water. In such cases, standard force fields will fail and force fields specific for tackling such interactions must be used.<sup>[64–67]</sup> When dealing with small adsorbate molecules (e.g., methane, nitrogen, carbon dioxide), it is also usual to treat them as rigid models for computational simplicity. However, for larger molecules like long alkanes, bonded interactions (stretching, bending, and torsion) play an important role and special techniques like configurational bias<sup>[68]</sup> can be used to speed up the sampling. Due to the use of periodic boundary conditions (which are standard in classical molecular simulations), GCMC is particularly suited to describe crystalline materials like MOFs or zeolites, which are inherently periodic. However, this method can also be used to study semi-crystalline or even completely amorphous materials, although in these cases, particular care must be taken to sample multiple realizations of each material structure so as to adequately sample the degree of structural variability observed in the real materials (see next Section).

## 2.4. CarbGen Tool for Activated Carbon Model Generation

Optimization of activated carbons is an open topic of scientific interest, with most efforts geared toward surface functional group content optimization and/or microporous structure tuning,<sup>[69]</sup> because they are potential materials for application in, for example, water treatment, heavy metal recovery, air purification, and catalysis.<sup>[70]</sup> In recent years, computational modelling of such materials has experienced a boom in development.<sup>[71,72]</sup> Given the amorphous nature and highly irregular structural organization of activated carbons, modeling real-world examples in silico is not trivial. An interesting approach is the usage of virtual porous carbon models. In such a model, activated carbons are represented as a set of micro crystallites grouped together to form a microporous structure.<sup>[73,74]</sup> The employed library of micro crystallites can be fine-tuned to reflect surface area, elemental composition, and even surface functional group content of differ-

ent activated carbon samples, reproducing experimental results with high-enough accuracy for computational optimization.

As a way to speed up and standardize the generation of such micro crystallite libraries (with different chemical and physical properties), the CarbGen tool was developed.<sup>[75]</sup> This tool is freely available on a web server,<sup>[76]</sup> and as an open-source Python standalone version.<sup>[77]</sup> As shown in **Figure 2**, the online tool allows for easy generation of multiple replicas of functionalized carbon models in an extremely simplified way. More recently, as part of the ProtoSyn.jl package,<sup>[78]</sup> the same approach was improved with the addition of 4 new nitrogen-containing functional groups and a multitude of tools for more accurate generation of models (for example, introducing the option to quickly minimize the structure and solve atomic clash conflicts). The full code can be accessed in the Materials module of ProtoSyn.jl.<sup>[78]</sup>

## 2.5. Machine Learning

The application of machine learning (ML) for the study of materials aims primarily to screen or design new applied materials by developing systematic and high-throughput algorithmic frameworks.<sup>[79,80]</sup> Python or R programming languages are the main tools for machine learning in general, but KNIME and MATLAB are also widely used when dealing with materials, and a myriad of low- and no-code solutions are becoming increasingly available.

A machine learning workflow usually involves 5 steps, as described in the following sub-sections:

### 2.5.1. Data Preparation

To produce a machine learning model, it is necessary to have data to calibrate and evaluate it. Therefore, it requires the availability or collection of a database, which can range from a few dozen to millions of data entries. Then, the data need to be loaded, examined, processed, and cleaned. Cleaning involves dealing with missing data, different sources of errors and unit standardization. It is usually followed by exploratory data analysis, to discover correlations, spot anomalies, and test hypotheses, using complementary summary statistics and graphical visualization, in order to subsequently choose the appropriate machine learning approach. Often, when the term machine learning is heard, an alluring image of futuristic artificial intelligence applications is evoked. In reality, most of the time in a machine learning project is spent preparing data for the machine learning model.

### 2.5.2. Splitting Data into Train/Validation/Test Data Sets

The data should be divided into three data sets (training, validation, and test) in order to properly evaluate the performance of the model. The training set is used to fit a certain algorithm to find the model parameters, which are internal values that allow a model to make predictions. The validation set is then used to evaluate the choice of the algorithm and respective hyperparameters. The hyperparameters are external values to the model, related to the training process, which can be chosen and tuned. In order to reduce the bias to the validation set, *n*-fold cross-validation

**CarbGen**

Molecular modelling of carbon based materials has shown promising results in the search for molecular mechanisms of various interactions. One of the challenges of creating these models is the correct incorporation of functional groups in a quantitative fashion, with proper definition of atom types and charges in topology files. CarbGEN is a new computational tool, allowing free and easy design of functionalized carbon materials with complex microporosity detail.

For more details, please consult the associated [reference](#).

**Functionalizations**  
The amount of each functionalization type attached to carbon atoms, given as percentage

Carbonyls: 9 %      Carboxyls: 5 %  
Ethers: 25 %      H-termini: 50 %

**Residue size**

Size: 10 rings (number of rings in the x and y directions (Max: 25))  
Layers: 1 layers (number of layers (Max: 5))  
Porosity: 10 level (microporosity level (From 0 to 10))

**Output**

**TIP!** Consider using multiple replicas, convert the .top files to .itp and insert them into a single simulation box.  
Replicas: 1 (Max: 5)      **Generate**

**TIP!** Hit copy to reuse the parameters used to create this example      **Copy**

**Examples**  
Cycle through different examples. Try to rotate the carbon model for a better view

Single layer of functionalized oxide-graphene

itp for GROMACS simulation

**Figure 2.** CarbGen Online tool. a) A percentage of functionalized carbon atoms can be set for the various types of commonly found functional groups. These settings reflect the surface chemistry of the final model. b) The physical characteristics of a micro crystallite include its size, number of layers, and porosity level. These settings modulate the micro porosity of the final model. c) Examples and templates allow for a quick copy of commonly found micro crystallite types in the literature. The downloadable output includes a description of the generated model (elemental composition, functional group content, etc.), a .mol2 file with the default atomic charges and an .itp file with force field parameters for molecular dynamics simulation using the GROMACS software.

should be employed, with  $n$  recommended to be 5 or 10.<sup>[81]</sup> Both result in similar low bias toward the validation sample and equal mean square error for different methods and test sets.<sup>[81]</sup> In ten-fold cross-validation, for example, a model is evaluated 10-times against ten independent samples corresponding to 10% of the dataset after it is trained 10 different times with the remaining 90% of the validation data.

The test set should be held out from the feature selection, training, optimization, and validation stages, being stored for a final independent test of the most accurate model according to cross-validation. The amount of data reserved for the test set is usually between 10% and 30% of the whole dataset, depending on the amount of data available and the nature of the problem. If the performance of the model toward the test set is not satisfactory

and the model needs to be further refined, new pristine data (not present in the initial training, validation, or test sets) should be used for further testing.

### 2.5.3. Feature Engineering

Features are independent variables that are used as an input for the model to predict an intended output. For materials design, they are also referred as descriptors; it can be any relevant characteristic of the material, such as measured experimental properties, tabulated properties, and/or calculated properties obtained by DFT, MD, or cheminformatics. For numerical problems involving materials, finding the features with higher predictive

power is often more important than the choice of algorithm,<sup>[8]</sup> and expert knowledge is usually key. In the case of materials properties, the number of possible features is generally very broad, so statistical techniques for feature selection are employed.<sup>[82]</sup> There are filter methods, based on filtering according to a certain score from different statistical tests for the correlation between features and outcome variables, there are the so-called wrapper methods, such as backward elimination and forward selection, and algorithms that have their own built-in feature selection methods, such as the least absolute shrinkage and selection operator (LASSO) regression. No method can be considered the best for all problems, and this step can be repeated several times considering different strategies.<sup>[82]</sup> It is common in problems involving materials to have initially hundreds or even thousands of features, from which only one or two dozen are typically selected for model optimization. During the model optimization step, the selected features can be further refined using ML models with optimized hyperparameters.

#### 2.5.4. Model Optimization

There are many different algorithms that can be used to develop machine learning models. First, it is necessary to identify the right machine learning task: unsupervised learning versus supervised learning. Unsupervised learning can be used on unlabeled raw data and is used to unveil relationships and patterns within this data, whereas supervised learning requires labeled data and is used to make predictions on new data.

Unsupervised learning relies on clustering, which groups together similar data points, or association techniques, which allow to understand how different features are related with each other. On the other hand, supervised learning usually addresses two different problems: Regression, which aims to predict numerical outcomes (i.e., the value of a property), and classification, which aims to identify discrete classes of data (i.e., efficient vs non-efficient material according to a certain criteria or threshold). Most well-known supervised learning algorithms can be used for both regression and classification. These can be, for example, regression (simple linear, multiple, LASSO, Ridge), *k*-nearest neighbors, simple decision trees, or with ensemble methods (random forests, bagging, XGBoost), support vector machines and deep learning. The majority of these algorithms were described in previous work.<sup>[83]</sup> For standard tabular data, XGboost is usually the best performing algorithm,<sup>[84]</sup> although it can be cumbersome to find the optimal hyperparameters and simpler algorithms generally offer higher explanatory power.<sup>[85]</sup> On the other hand, deep learning really shines when dealing with images, audio, and text.<sup>[84]</sup>

The objective of model optimization is to find the ideal combination of algorithm, model parameters, and training hyperparameters, according to the performance metrics obtained from cross-validation. There are two main problems with machine learning models: Underfitting and overfitting. Underfitting means that a model does not fit well enough the training data and thus generalizes poorly to the validation and testing data. Overfitting means that a model fits so well to the training data that it becomes too specific to this data and has difficulty generalizing for the validation and training sets. Underfitting is relatively

easy to spot, while cross-validation helps minimize overfitting. However, cross-validation does not completely prevent overfitting, with materials science being quite prone to this problem. Experimental materials science, especially for high performance applications, has relatively small datasets, sometimes even smaller than the number of features that are possible to consider, which together with many algorithms to choose from and numerous hyperparameters to tune, can result in a chosen final model that is actually specific to the cross-validation itself, not generalizing well to the test set.

#### 2.5.5. Testing

The final test set allows the assessment of the real performance of the model. Moreover, since new data are always being published or it is relatively easy to collaborate with other labs to obtain new data, an additional blank test set with external data can also be considered to evaluate the model.

### 3. Computational Studies of Materials

#### 3.1. Metal Organic Frameworks

MOFs are hybrid porous materials composed of inorganic metal ions or ion clusters linked together by organic moieties (usually named ligands or linkers), typically in a 3D crystalline structure.<sup>[86]</sup> The coordination of the metal controls how many organic linkers can be bound to the metal and their orientation, and organic linkers shape the skeleton of the material.<sup>[87]</sup> MOFs can have many different geometries, with surface areas ranging from 1000 to 10 000 m<sup>2</sup> g<sup>-1</sup> and porosities going above 50% of the volume of the structure, and some exhibit high thermal and chemical stability.<sup>[86]</sup> Another main feature of MOFs is their tunability: On a first level, there are infinite possible combinations of different metals and organic linkers; on a second level, post-synthetic functionalization or structural phenomena such as interpenetration (i.e., the merging of more than one independent framework in the same structure) add more numbers to the exponentially growing list of reported MOFs, which to date counts over 100 000 structures in the Cambridge Structural Database (CSD).<sup>[88]</sup> All of these characteristics turn MOFs into one of the most versatile types of porous materials; as they can be tailored for specific uses, applications spread over many different fields including adsorptive gas separation,<sup>[89]</sup> carbon capture,<sup>[90]</sup> catalysis,<sup>[91]</sup> sensing,<sup>[92]</sup> energy storage and conversion,<sup>[93]</sup> pollutant removal,<sup>[94]</sup> and drug delivery.<sup>[95]</sup>

Because there are countless possible MOFs, it is not feasible to synthesize and test all of them experimentally for specific applications. Hence, computer simulations provide excellent tools to further study and screen these materials.<sup>[96]</sup> Computer simulations allow the achievement of a deep molecular-level understanding of the mechanisms governing host-guest interactions, the testing of possible structural and/or chemical changes in the frameworks and the development of models based on experimental data, that will enable studies under conditions not possible experimentally. However, there may also be some drawbacks: computational approaches and models may not be accurate enough to represent

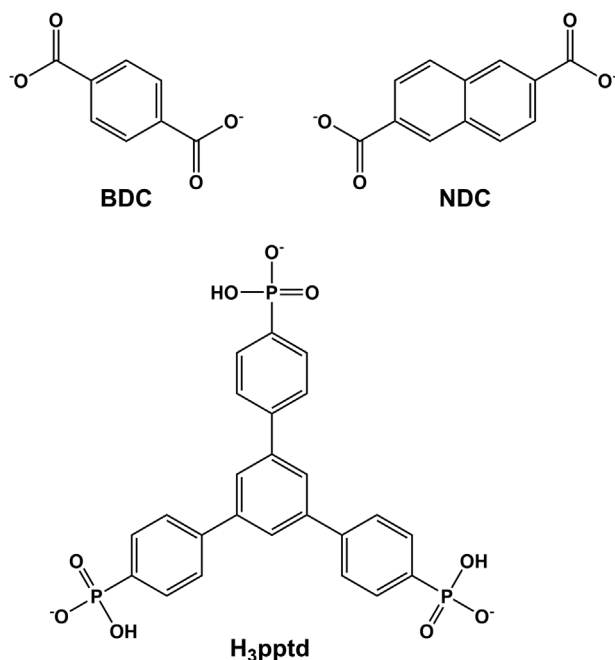


**Figure 3.** Structures of the linkers in the MOFs discussed in the text which were obtained from 1,4-benzenedicarboxylic acid (top left), 2,6-naphthalenedicarboxylic acid (top right), and 1,3,5-tris(4-phosphonophenyl)benzene (bottom) parent compounds.

the system being studied; some experimental samples may be difficult to properly describe computationally, namely due to defects or impurities, not always obvious to implement on the perfect structures of MOFs.<sup>[87]</sup> Nevertheless, computational simulations are a fundamental step in the research process in materials science and engineering.

Our group has been studying MOFs for more than a decade, with our computational research focusing on modelling the adsorption of small gas molecules in MOFs with different structural and chemical properties.<sup>[100–102,65–67,97–99]</sup> Recently, we participated in the investigation of the multifunctionality of an ion-exchanged rare-earth-phosphonate MOF.<sup>[102]</sup> The MOF, built of phosphonate-based tripodal organic linkers (H<sub>3</sub>pptd, **Figure 3**) and rare-earth/lanthanide cations (95% Yttrium, 5% Europium), labelled 1\_Eu, was modified by post-synthetic ion-exchange to replace the protons (H<sup>+</sup>) of the free –POH groups with extraframework potassium cations (K<sup>+</sup>), 1K\_Eu. Computer simulations of the adsorption of several small gas molecules, including carbon dioxide (CO<sub>2</sub>), acetylene (C<sub>2</sub>H<sub>2</sub>), propylene (C<sub>3</sub>H<sub>6</sub>) and propane (C<sub>3</sub>H<sub>8</sub>), in 1\_Eu and 1K\_Eu, helped to further understand the structure of the materials and their interactions with the gases. Starting from the experimental crystallographic cell obtained for 1\_Eu, with H<sup>+</sup> replaced by K<sup>+</sup> for 1K\_Eu, both MOF structures were optimized by DFT, with GCMC simulations having been run to calculate CO<sub>2</sub> adsorption isotherms at 298.15 K. The calculated adsorption isotherms for both materials have corroborated experimental findings, i.e. that there is a significant increase in CO<sub>2</sub> uptake in 1K\_Eu in comparison with 1\_Eu, due to the stronger interactions of the gas in the former's chemical environment. The calculated results consistently overestimated the adsorbed amounts, a fact that has been attributed to the dif-

ferences between the simulated (i.e., perfect) structure and the experimental defective material. These quantitative differences notwithstanding, this was seen as a good indicator that 1K\_Eu and 1\_Eu had very similar structures, a fact that could not be fully clarified experimentally. CO<sub>2</sub> density plots obtained from GCMC calculations for 1\_Eu and 1K\_Eu have also helped to identify the preferential CO<sub>2</sub> adsorption regions for both materials: near the organic linkers for the former and near the exchanged K<sup>+</sup> for the latter. Additional DFT calculations were also performed to determine the adsorption energies of CO<sub>2</sub>, C<sub>2</sub>H<sub>2</sub>, C<sub>3</sub>H<sub>6</sub>, and C<sub>3</sub>H<sub>8</sub> and the most favorable adsorption arrangements of the guest molecules.

The separation of gas mixtures is a common industrial practice. However, some gas mixtures are inherently difficult to separate because their components have very similar properties. One such example is the separation of ethane/ethylene (C<sub>2</sub>H<sub>6</sub>/C<sub>2</sub>H<sub>4</sub>) mixtures, one of the most important and challenging industrial separations due to the significance of C<sub>2</sub>H<sub>4</sub> as a primary feedstock in the petrochemical industry. Because of the close boiling point of both compounds in cryogenic conditions, traditional distillation-based methods are highly energy intensive processes and, consequently, very costly. Adsorption-based processes, in which a porous material preferentially adsorbs one of the components in the gas mixture over the other(s), can be a viable alternative, especially if the material is selective toward C<sub>2</sub>H<sub>6</sub>.<sup>[103,99]</sup> Over the past years, our group has studied several types of MOFs that have interesting characteristics for C<sub>2</sub>H<sub>6</sub>/C<sub>2</sub>H<sub>4</sub> separation.<sup>[100,99]</sup> In one of these works, we studied zirconium (Zr) MOFs based on UiO-66 and MIL-140, with different structures and chemical functionalities.<sup>[100]</sup> All structures considered for these computational studies were optimized by DFT, while GCMC was used to obtain adsorption isotherms. UiO-based materials are built from discrete Zr<sub>6</sub> oxoclusters resulting in a 3D pore system with smaller tetrahedral and larger octahedral cages; MIL-140-based MOFs consist of infinite Zr oxide rods, originating structures with 1D triangular-shaped straight channels.

The first aspects to be investigated were the effect of the pore structure and linker aromaticity. For this, four MOFs were studied: two UiO-based and two MIL-140-based MOFs, with 1,4-benzenedicarboxylate (BDC, **Figure 3**, yielding UiO-66 and MIL-140A, respectively), or 2,6-naphthalenedicarboxylate (NDC, **Figure 3**, yielding UiO-NDC and MIL-140B, respectively) organic linkers. BDC-containing structures have smaller pore dimensions (and consequently, lower pore volumes and surface areas) and lower aromaticity than NDC-containing MOFs. The calculated adsorption isotherms, which were in general agreement with the experimental ones, and the analysis of the preferential adsorption locations supported the following findings: i) Regarding the topology of the structures, UiO-based MOFs adsorb more gas and have a higher affinity for C<sub>2</sub>H<sub>6</sub> over C<sub>2</sub>H<sub>4</sub> than MIL-140-based materials, with UiO-NDC showing the highest uptakes for both gases. This was attributed to the 3D tetrahedral and octahedral cages of the UiO-based materials, as opposed to the 1D channels of the MIL-140 based MOFs; ii) Considering the aromaticity of the organic linker, it was observed that a higher aromaticity seems to lead to enhanced interactions with C<sub>2</sub>H<sub>6</sub>, as MOFs with NDC were shown to adsorb (to different extents) more C<sub>2</sub>H<sub>6</sub> than C<sub>2</sub>H<sub>4</sub>. However, in the case of UiO-based MOFs, the C<sub>2</sub>H<sub>6</sub>/C<sub>2</sub>H<sub>4</sub> selectivity estimated from both experimental and simulated



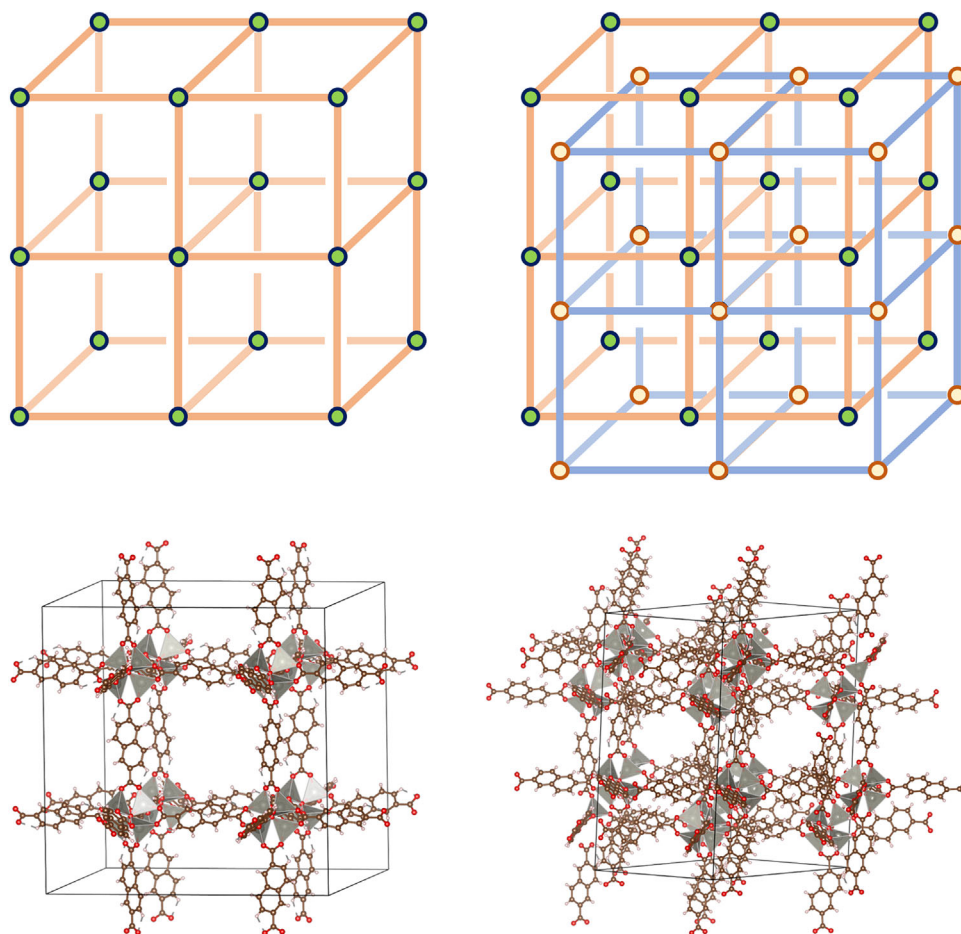


**Figure 4.** Schematic (top) and ball-and-stick/polyhedra (bottom) representations of IRMOF-8 without (left) and with (right) interpenetrated structure. In the top images, spheres and lines represent the zinc-oxide clusters of the inorganic nodes and the NDC organic linkers, respectively. In the bottom images, drawn with VESTA,<sup>[104]</sup> gray is Zn, red is O, brown is C, and white is H. In the top-right image, two different coloring schemes are used to highlight the two cages.

results for UiO-NDC was lower than for UiO-66. This suggested that the aromaticity in these structures may not have had a significant effect on the separation of the gases (under the conditions tested), and that the observed high gas uptakes in UiO-NDC could in fact be due to the bigger pores of this MOF, and consequent higher pore volume and surface area, than UiO-66.

Density plots for  $C_2H_6$  and  $C_2H_4$  adsorption taken from GCMC simulations were important in identifying preferential adsorption sites and better understanding the effect of the topology and aromaticity: For UiO-66 and UiO-NDC the preferential adsorption sites were found to be in tetrahedral cages where the organic linkers face the interior of the pores; for MIL-140A and MIL-140B the adsorption inside the 1D channels is made difficult not only by the narrow pore size but also by directional constraints and the misalignment of the linkers facing the inside of the channels. Linker functionality was also investigated. After promising experimental adsorption results showed UiO-66- $2CF_3$  (identical to UiO-66 but in which BDC linkers have a  $CF_3$  group in positions 2 and 5) to be highly selective toward  $C_2H_6$ , a more detailed computational study of this material was conducted to better understand the adsorption process and evalu-

ate the influence of linker dihedral rotation (relative to the metal clusters) on the selectivity of the material. Different configurations were tested and results clearly showed that linker rotation, which affects pore size and configuration, has a significant influence on  $C_2H_6$  and  $C_2H_4$  adsorption. By comparison with experimental results, these simulated adsorption isotherms revealed a complex adsorption mechanism: The adsorption of the two gases is accompanied by changes in linker rotation with increasing gas pressures, that ultimately favors  $C_2H_6$  adsorption over  $C_2H_4$ .

In another study, we investigated the adsorption behaviors of  $C_2H_6$ ,  $C_2H_4$ , and also methane ( $CH_4$ ) and  $CO_2$  in zinc (Zn) based isorecticular (IR) MOFs.<sup>[99]</sup> The focus of this study was IRMOF-8, which was shown to be more selective toward  $C_2H_6$  than  $C_2H_4$  in experimental studies,<sup>[105]</sup> and thus a good candidate for this separation. IRMOF-8 may present non-interpenetrated (IRMOF-8-NOINT) or interpenetrated (IRMOF-8-INT) structures (**Figure 4**). Because of the structural interpenetration, the latter form has a smaller pore volume than the former. For all gases, simulated adsorption isotherms for IRMOF-8-INT showed a closer fit to experimental isotherms, indicating that the synthesized material had a high degree of interpenetration. It should be noted that for

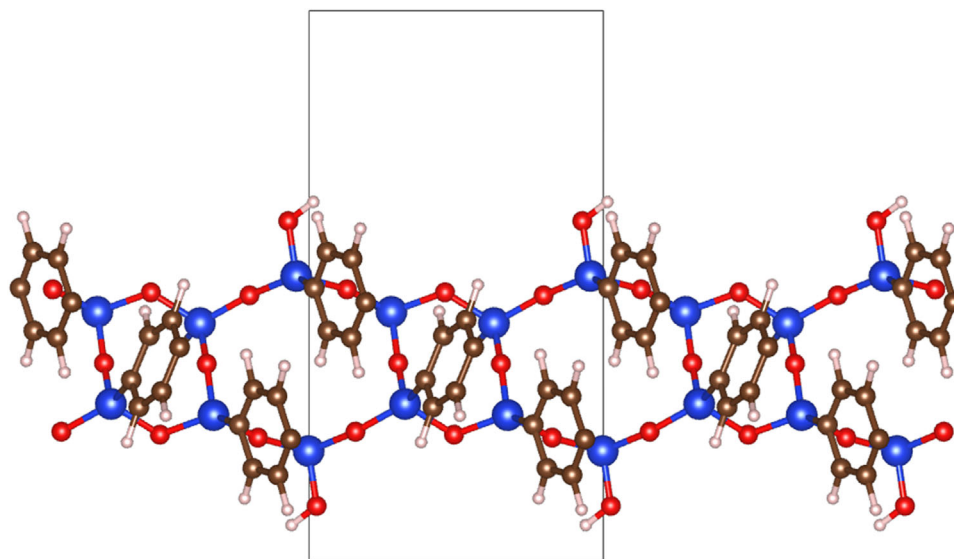


**Figure 5.** Ball-and-stick representation of the periodic phenylene-PMO model drawn with VESTA.<sup>[104]</sup> Color code: blue is Si, red is O, brown is C, and white is H. The black rectangle defines the unit cell, with its size in the perpendicular direction reduced for clarity of representation.

$C_2H_6$  and  $C_2H_4$  adsorption, non-polar and point charge models were tested for both gases and that the simulated isotherms for both models overlapped, suggesting that Coulombic interactions were not influencing gas uptake. Consequently, we concluded that the selective adsorption of  $C_2H_6$  over  $C_2H_4$  in IRMOF-8-INT was associated with van der Waals interactions, which are slightly stronger for  $C_2H_6$  than for  $C_2H_4$ .

Occupancy maps taken from simulation results shed further light into the adsorption mechanism of these gases: For pressures below 100 kPa,  $C_2H_6$  and  $C_2H_4$  adsorption occurs in the vicinity of the inorganic nodes of IRMOF-8-INT, and as pressure increases occupancy progressively builds around the organic linkers. Additional simulations in a canonical ensemble (NVT) with just one  $C_2H_6$  or  $C_2H_4$  molecule allowed us to locate the preferential adsorption sites in IRMOF-8-INT to be within the aromatic linkers of the two different cages. The simulations run for IRMOF-8-INT showed that  $C_2H_6$  and  $C_2H_4$  uptakes are much higher and lower at low and high pressures, respectively, than in IRMOF-8-NOINT. This is also due to interpenetration. IRMOF-8-INT has lower pore volume and surface area but a higher density of organic linkers per volume than IRMOF-8-NOINT. Thus, at low pressures, where adsorption is governed by framework-adsorbate interactions, van der Waals interactions are much stronger in the former than in the latter. At high pressures, where adsorbate-adsorbate interactions are more significant, the larger pores of IRMOF-8-NOINT lead to much higher gas uptakes. For  $CH_4$  and  $CO_2$ , simulated results were also in agreement with experimental data, although slightly overestimated in the latter.

### 3.2. Periodic Mesoporous Organosilicas

Periodic mesoporous organosilicas (PMO), discovered in 1999,<sup>[106–108]</sup> are mesoporous 2D structures formed by bisilylated organic bridges ( $((R'O)_3Si-R-Si(OR')_3$ ,  $R'$  = methyl or

ethyl,  $R$  = bridged organic group) linked to each other by silica moieties.<sup>[109,110]</sup> In this class of materials, the organic moieties are homogeneously distributed and directly integrated in the wall of the PMO, keeping the pore channel free for potential applications,<sup>[106–108,110,111]</sup> such as electronics, adsorption, storage and separation, and catalysis.<sup>[110]</sup> The most advantageous properties of this family of hybrid materials are related to its hydrophilic-hydrophobic character, narrow pore size distribution, highly ordered pore nature, large specific surface areas and pore volumes, tunable pore sizes, and free silanols that can be easily modified to incorporate extra functional groups.<sup>[110,111]</sup> Despite the high concentration of organic groups, PMO materials usually present higher thermal stability and moisture tolerance than MOFs and post-functionalized periodic mesoporous silicas (PMS) sorbents. It is the intercalation of organic/inorganic groups in the pore walls that enhances the stability of the material, and it is the combination of all these features that make PMO materials attractive as adsorbents.

DFT was used to understand and predict the performance of a variety of PMO materials displaying different chemical functionalities, mainly for  $CO_2$  and  $CH_4$  adsorption/separation<sup>[112–115]</sup> but also for separation of  $CO_2$  from other gases.<sup>[116]</sup> Both periodic<sup>[112–114]</sup> and cluster models<sup>[115,116]</sup> of the PMO walls were considered to perform those studies, which were based on the sequence of six- and four-member rings of organosilica with  $T^3$  to  $T^2$  silicon environments, that is,  $T^n = RSi(OH)_{(3-n)}(OSi)_n$ , where  $R$  represents the organic bridge, in a ratio of 2:1, as used for the first time by Martinez and Pacchioni<sup>[112]</sup> to construct the periodic model of the phenylene (Ph-) PMO (Figure 5) based on information from solid-state NMR obtained by Comotti et al.<sup>[117]</sup>

The  $CO_2$  and  $CH_4$  adsorption performances, calculated using periodic models of the functionalized and pristine Ph-PMO sorbents,<sup>[113,114]</sup> showed a good agreement with the obtained experimental adsorption data, as discussed below. However, PMO-based cluster models<sup>[116]</sup> are very convenient because they are computationally affordable when compared with the periodic

**Table 1.** Energies, selected geometrical parameters and CO<sub>2</sub>/CH<sub>4</sub> selectivity for CO<sub>2</sub> and CH<sub>4</sub> adsorption in the periodic and cluster models of Ph-PMO calculated using different methods.

Gas	Model <sup>a)</sup>	DFT method	$E_{\text{ads}}$ (kJ·mol <sup>-1</sup> )	Dist(X...HO) <sup>b)</sup> (Å)	Dist(C...Ph <sub>center</sub> ) <sup>c)</sup> (Å)	$E_{\text{ads}}^{\text{CO}_2}/E_{\text{ads}}^{\text{CH}_4}$ <sup>d)</sup> ratio	
CO <sub>2</sub>	Periodic	PBE	-10.9	2.28	6.60	2.15	
		PW/PAW	PBE-D2	-21.7	2.26	6.34	2.24
	Cluster	PBE	-10.5	2.22	5.41	2.69	
		GTO	PBE-D2	-25.8	2.21	5.18	1.79
		M06-2X	-25.1	2.21	5.17	2.46	
	Experimental <sup>e)</sup> / <sup>f)</sup>			-19			3.2 <sup>g)</sup>
	$\Delta H^i)$ (kJ·mol <sup>-1</sup> )			-20.4			
$\Delta S^j)$ (kJ·mol <sup>-1</sup> ·K)			-126.5				
CH <sub>4</sub>	Periodic	PBE	-5.7	5.39	5.79		
		PW/PAW	PBE-D2	-13.1	5.36	5.78	
	Cluster	PBE	-10.1 <sup>h)</sup>	2.11 <sup>h)</sup>	8.16 <sup>h)</sup>		
		GTO	PBE-D2	-3.9	2.24	6.42	
		M06-2X	-14.4	2.56	4.88		
	Experimental <sup>e)</sup> / <sup>i)</sup>			-12.6 ± 0.8			
	$\Delta H^j)$ (kJ·mol <sup>-1</sup> )			-4.5			
$\Delta S^j)$ (kJ·mol <sup>-1</sup> ·K)			-100.7				

<sup>a)</sup> PW/PAW and GTO stand for plane-wave/projected-augmented wave and Gaussian type orbitals, respectively; <sup>b)</sup> Nearest-neighbor distance between the adsorbate (X = O or H for CO<sub>2</sub> and CH<sub>4</sub>, respectively) and the hydrogen atom of the isolated T<sup>2</sup> silanol group (compare Figure 1 in ref. [116]); <sup>c)</sup> Distance from the carbon atom of the adsorbate to the center of the aromatic ring of the PMO (compare Figure 1 in ref. [116]); <sup>d)</sup> Ratio between the calculated adsorption energies of CO<sub>2</sub> and CH<sub>4</sub>; <sup>e)</sup> Experimental isosteric heat of adsorption; <sup>f)</sup> From adsorption isotherms (temperatures, pressure range, and uncertainty not specified) in ref. [117]; <sup>g)</sup> Ratio of Henry's constant for CO<sub>2</sub> to that for CH<sub>4</sub> determined in ref. [114]; <sup>h)</sup> Second most stable structure for PBE-D2 method; <sup>i)</sup> From adsorption isotherms at  $T = 285, 298,$  and  $314$  K and pressures of 0.01 to 0.1 MPa determined in ref. [118]; <sup>j)</sup> Enthalpies and entropies associated with the reaction Gas + Ph-PMO → Gas...Ph-PMO with thermal corrections to the energy obtained from M06-2X/6-31G\*\* (unscaled) frequency calculations at  $T = 298.15$  K.

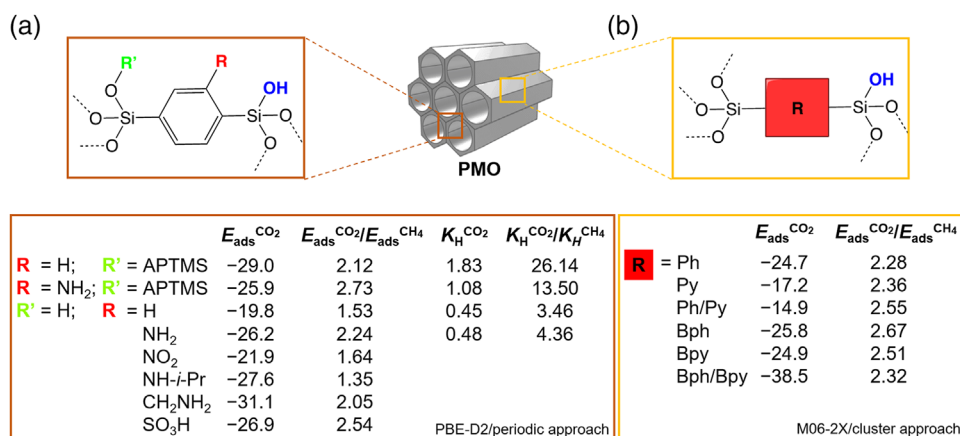


**Figure 6.** Schematic representation of a) R- and R'- post-functionalized Ph-PMOs studied in ref. [114] and b) PMOs with different organic bridges (Ph, Py, Bph, and Bpy denotes phenylene, pyridine, biphenylene, and bipyridine moieties, respectively) considered in ref. [115].  $E_{\text{ads}}^{\text{CO}_2}$ ,  $E_{\text{ads}}^{\text{CH}_4}$ ,  $K_{\text{H}}^{\text{CO}_2}$  and  $K_{\text{H}}^{\text{CH}_4}$  are the calculated CO<sub>2</sub> adsorption energy, the CH<sub>4</sub> adsorption energy, the Henry constant for CO<sub>2</sub> and the Henry constant for CH<sub>4</sub>, respectively.  $E_{\text{ads}}$  and  $k_{\text{H}}$  are presented in kJ mol<sup>-1</sup> and mmol·g<sup>-1</sup>·kPa<sup>-1</sup> × 10<sup>-2</sup>, respectively. The ratio of the Henry constant for CO<sub>2</sub> and CH<sub>4</sub> ( $K_{\text{H}}^{\text{CO}_2}/K_{\text{H}}^{\text{CH}_4}$ ) is equivalent to the selectivity in the limit of zero coverage.

models and can deliver accurate energetic data for the interaction of these two adsorbates with the walls of the Ph-PMO material, as observed in Table 1, independently of the chosen DFT exchange-correlation functional.

The validation of cluster models allowed the extension of this kind of studies to the adsorption of other gaseous molecules (e.g., diatomic CO, H<sub>2</sub>, N<sub>2</sub>, O<sub>2</sub>, and NO, the triatomic CO<sub>2</sub>, H<sub>2</sub>O, H<sub>2</sub>S,

and SO<sub>2</sub>, and the tetratomic SO<sub>3</sub> and NH<sub>3</sub> species) onto the Ph-PMO pore wall surface,<sup>[116]</sup> as well as to study PMO sorbents with biphenylene (Bph-), pyridine (Py-), and bipyridine (Bpy-) bridges or mixtures of Ph/Py- and Bph/Bpy- moieties<sup>[115]</sup> as bridges (Figure 6).

Independently of the type of chemical functionalities introduced, DFT studies demonstrated that CO<sub>2</sub> is preferentially ad-

sorbed over CH<sub>4</sub> on Ph-PMOs, making this family of materials interesting to separate CO<sub>2</sub> from CH<sub>4</sub> (Table 1 and Figure 6). Also, it was found that both gases are physisorbed on the PMO walls, which is advantageous for the adsorbent regeneration. In the case of Ph-PMO<sup>[112–116]</sup> and Bph-PMO<sup>[115]</sup> sorbents, the favored adsorption sites are the isolated T<sup>2</sup> type silanol species. Moreover, for the Ph-PMO a clear correlation was observed between the calculated adsorption energies ( $E_{\text{ads}}$ ) and the adsorbate to adsorbent distances (Dist(X⋯HO) and Dist(C⋯Ph<sub>center</sub>)) or the experimental proton affinities ( $E_{\text{pa}}$ ) of CO<sub>2</sub>, CH<sub>4</sub>, and of the diatomic, triatomic and tetratomic molecules. The latter relationship is convenient to quickly evaluate the adsorption of other gases on the walls of the Ph-PMO sorbent.<sup>[116]</sup>

When amines are introduced into the Ph-PMO material (Figure 6a), DFT calculations employing periodic models and experimental gas adsorption measurements predict an increase of the CO<sub>2</sub> adsorption energy, Henry constant for CO<sub>2</sub> and CO<sub>2</sub>/CH<sub>4</sub> selectivity ( $K_{\text{H}}^{\text{CO}_2}/K_{\text{H}}^{\text{CH}_4}$ ), with a good correlation between calculated and experimental data.<sup>[114]</sup> Moreover, it was demonstrated that the PMO functionalized with alkyl amines (APTMS@Ph-PMO) interacts more favorably with CO<sub>2</sub> than the PMO modified with aromatic amines (NH<sub>2</sub>-Ph-PMO). In fact, it was concluded that the CO<sub>2</sub> sorption affinity is more controlled by the type of amine than by the nitrogen content in the PMO channels. As both DFT calculations and experimental studies showed the same adsorption-separation trend, theoretical studies were also used to predict if other chemical modifications of the PMO (–NO<sub>2</sub>, –NH-*i*-Pr, –CH<sub>2</sub>NH<sub>2</sub>, and –SO<sub>3</sub>H) can enhance the selectivity of CO<sub>2</sub> over CH<sub>4</sub>. The Ph-PMO modified with CH<sub>2</sub>NH<sub>2</sub> appeared to improve the CO<sub>2</sub> adsorption and the CO<sub>2</sub>/CH<sub>4</sub> selectivity.<sup>[114]</sup>

The effects of the organic bridge on the selectivity for CO<sub>2</sub> over CH<sub>4</sub> were also studied by DFT (Figure 6b).<sup>[115]</sup> Cluster models of the walls of the PMO materials with the organic Ph- bridge replaced by Py-, Bpy-, or Bph- moieties, or by mixtures of Ph/Py- and Bph/Bpy- fragments, were considered. Notably, improved CO<sub>2</sub> adsorption was observed when Bpy-bridges were mixed with Bph- moieties, while the Bph- bridge led to a similar behavior as the parent Ph-PMO. Curiously, the Bpy/Bph-PMO is predicted to be the least interesting material for CO<sub>2</sub>/CH<sub>4</sub> separation since the selectivity toward CO<sub>2</sub> decreased slightly, while it increased in all the other cases analyzed. The CO<sub>2</sub> adsorption performance was directly correlated to the SiOH⋯OCO distance, namely, the adsorption strength was enhanced with the shrinkage of this distance. Py- and Ph/Py- PMO sorbents showed the lowest CH<sub>4</sub> adsorption energies.<sup>[115]</sup>

### 3.3. Periodic Mesoporous Silicas

PMS materials have gathered attention in many areas of investigation, e.g., in materials science or in the chemical and pharmaceutical industry,<sup>[119]</sup> due to their tunable properties, since the pore size, shape, or chemical speciation can be modelled by adjusting the synthesis conditions. The archetypal PMS material is the honeycomb-structured MCM-41 mesoporous silica, firstly synthesized by the Mobil oil company in 1992.<sup>[120]</sup> The mechanism behind the synthesis of MCM-41 has baffled researchers for several decades, since some stages are not com-

pletely understood. This stems from the complexity of the synthesis, where surfactant self-assembly, solvation, silica polymerization and phase equilibrium take place simultaneously, making their characterization a very challenging task for experimentalists and theoreticians alike. Based on indirect experimental evidence, two alternative mechanisms were proposed for the synthesis starting from an aqueous solution of CTAB surfactant and tetra ethyl orthosilicates (monomeric silica source): i) A liquid-crystal templating route, where silica plays a passive role by condensing around an already formed CTAB liquid crystal phase; ii) a cooperative templating mechanism, where, by contrast, silica plays a very active role in the templating mechanism by interacting closely with surfactant micelles and promoting the formation of the liquid crystal mesophase.<sup>[120,121]</sup> Despite extensive experimental work, several questions remained unanswered, mainly due to the difficulties in probing all stages of the synthesis mechanism in a systematic and consistent way.

Computational multiscale approaches, from quantum calculations to classical MC, MD, or dissipative particle dynamics simulations, provided remarkable insights into this mechanism at the nanoscopic scale. We implemented a multiscale strategy whereby an atomistic model of silicates was first developed<sup>[122,123]</sup> based on DFT calculations on a wide range of silicate species,<sup>[124]</sup> followed by parameterization of a coarse-grained MARTINI-based model for monomeric silica<sup>[37]</sup> in order to reach the time and length scales required to understand the early stages of the MCM-41 synthesis. The latter was benchmarked against experimental data, where possible, and against results obtained from previous AA-MD simulations.<sup>[122,123]</sup> Later, this CG model for monomeric silica was extended to cyclic and branched silica oligomers, with the goal of studying the mechanisms behind the synthesis of MCM-41 under realistic experimental conditions.<sup>[38]</sup> Diluted CTAB aqueous solutions comprising a wide range of concentrations of silica were used to analyze the impact of silica in the CTAB phase behavior. Chien et al.<sup>[125]</sup> characterized the phase behavior of CTAB aqueous solutions and the impact that silica monomers and dimers have on it. The picture emerging from these multiscale simulation studies is that monomeric silicate species interact very strongly with small surfactant micelles, leading to a sphere-to-rod transition.<sup>[37]</sup> However, on their own, silica monomers are unable to promote sufficient aggregation of micelles, requiring the presence of a minimum concentration of dimers (or larger oligomers) to act as a “glue” connecting different micelles together. This process quickly leads to the formation of a phase-separated hexagonal mesophase, under conditions that mimic the experimental MCM-41 synthesis carried out by Firouzi et al.<sup>[126]</sup> Crucially, the formation of the hexagonal MCM-41 mesophase only took place under the presence of silica oligomers, unequivocally supporting the cooperative templating mechanism (CTM) hypothesis. Furthermore, our CG model was able to reproduce other ordered structures at high CTAB concentration, such as the bicontinuous phase MCM-48 and the layered MCM-50, in agreement with experiments.<sup>[125]</sup>

In more recent work, this multiscale strategy has been extended to describe the synthesis of hexagonal mesoporous silica (HMS) materials, a close relative of MCM-41 but whose synthesis had been postulated to proceed through a neutral templating mechanism.<sup>[127]</sup> However, results from both simulations and experiments have disproved this mechanism,<sup>[128,129]</sup> demonstrat-

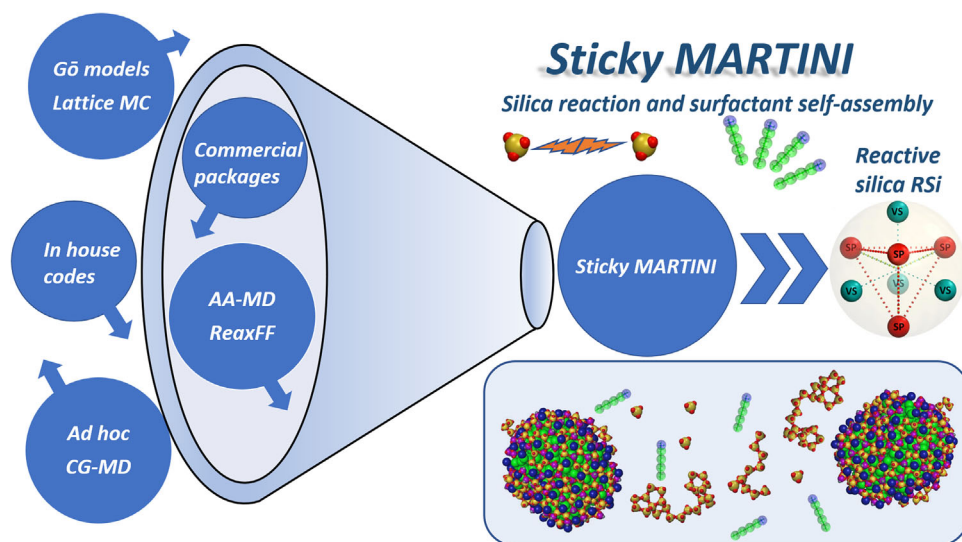


**Figure 7.** Scheme illustrating diverse literature computer simulations approaches to tackle chemical reactions and self-assembly of amphiphilic compounds. The Sticky MARTINI model with the novel RSi reactive silica surpassed most of the limitations of literature approaches.

ing instead that the formation of the hexagonal mesophase structure is driven by charge-matching interactions of similar nature to those present in the MCM-41 synthesis, even when the pH is lowered. A consequence of the lower pH in the HMS synthesis, however, is that the material becomes less ordered, partly explaining why it has not yet been possible to synthesize ordered PMS materials at neutral pH conditions.

Despite yielding unprecedented insight over the synthesis of PMS materials, the simulations described above suffer from an important drawback—the silica speciation had to be fixed at the beginning of each simulation, since silica polymerization reactions were not explicitly described in this model. More recently, we developed a new model that can not only model the surfactant self-assembly but also the simultaneous silica condensation reactions, preserving the essential advantages of the MARTINI framework, viz. simplicity, speed, computational efficiency, and transferability. Carvalho et al.<sup>[59]</sup> tackled this complicated task by incorporating virtual sites (VS) and “sticky” particles (SP) in the MARTINI beads in order to emulate the tetrahedral alignment of silica condensation and the geometry of the Si—O bonds and Si—O—Si angles.<sup>[59]</sup> In more detail, the reactive CG silicate model comprises a new  $S_{Si}$  bead surrounded by four VS and four SP establishing two tetrahedra in a stellated octahedron configuration—the so-called RSi (Reactive Silica)—for both neutral and deprotonated species (Figure 7). The Si—O—Si chemical bond formation and breakage was captured throughout a careful balance between attractive SP—SP interactions (mimicking the reaction itself) and repulsive VS—SP interactions (preventing overcoordination). Those two parameters were carefully calibrated by comparing the fraction of RSi that are bonded to “n” other RSi moieties as a function of time,<sup>[130]</sup> to analogous results obtained experimentally,<sup>[131]</sup> and from previous implicit solvent MC simulations.<sup>[132]</sup>

The calibrated model was then employed to evaluate the impact of silica oligomerization on the phase behavior of CTAB aqueous solutions. It was found that anionic silicate monomers are initially driven unreacted to the CTAB micelle by electrostatic

interactions. However, the high local silica concentration at the micelle surface then acts as a pseudo-catalyst to speed up the condensation reaction, a key step that further supports the CTM pathway.<sup>[120,121]</sup> The simulation then proceeded to yield a highly condensed silica shell surrounding the surfactant micelle, in a process reminiscent of silica hollow nanosphere formation. This initial study served as a proof-of-concept to demonstrate that the Sticky MARTINI model is able to simultaneously explore chemical reactions and self-assembly processes under realistic experimental conditions, which represents a major step forward in comparison with prior approaches (see Figure 7). Nevertheless, the model still suffers from some limitations, such as the inability to explicitly describe the formation of water during the condensation reaction, as well as leading to silica structures that are less dense than their experimental counterparts.<sup>[59]</sup> Work to address those limitations, as well as to extend the model to other systems where both chemical reactions and self-assembly are important, is currently ongoing.

### 3.4. Layered Double Hydroxides

Layered double hydroxides (LDHs) are clay-like nanostructured materials composed of stacked cationic layers with interlayers containing charge-compensating anions.<sup>[133]</sup> Their stacked structure is held together through a relatively weakly bound network of hydrogen bonds, electrostatic effects and dispersive forces, giving these materials an anion-exchange capacity that can be tailored for different host-guest applications. They can be synthesized in a relatively inexpensive and potentially recyclable manner, with the most common compositions having the general formula  $[M_{1-x}^{2+}M_x^{3+}(\text{OH})_2]^{x+}(\text{A}^{n-})_{x/n} \times m\text{H}_2\text{O}$ , where  $M^{2+}$  and  $M^{3+}$  are di- and trivalent cations, respectively,  $\text{A}^{n-}$  is an anion, and  $x$  is equal to the molar ratio  $M^{3+}/(M^{2+} + M^{3+})$ . Functional molecules in the anionic form can be loaded into LDHs and released by an external trigger, which can be the change of pH or the presence of a targeted species also in the anionic form.<sup>[134]</sup> At high pH, func-

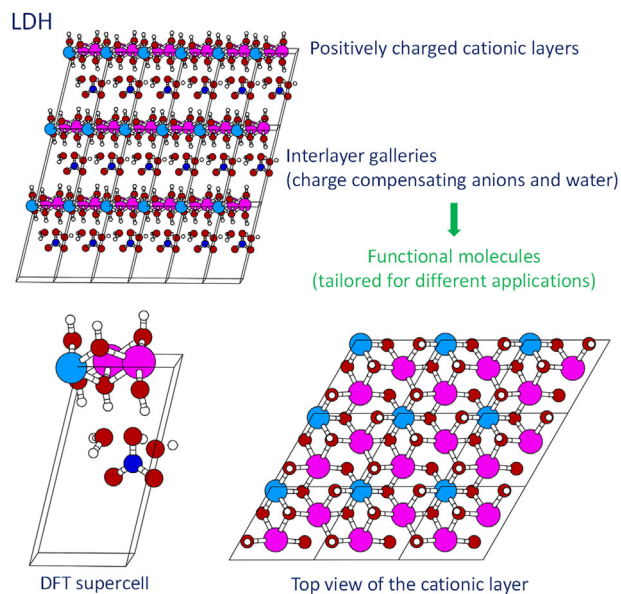


**Figure 8.** Typical LDH structure and features exemplified for a zinc–aluminum LDH with the nitrate anion intercalated. Color code: light blue is Al; pink is Zn; red is O; white is H; blue is N.

tional anions in the interlayer are exchanged by external hydroxyl anions, whereas at low pH the cationic layers dissolve, thus releasing the functional molecules from the interlayer. This mechanism also makes these materials well-known pH buffers, which can also be an important property for some applications, such as corrosion protection.<sup>[135]</sup> Moreover, the anionic exchange is not restricted to the hydroxyl anions from the pH changes, being also able to absorb targeted species, such as hazardous molecules from the environment.<sup>[136]</sup> This functionality makes them versatile functional materials for drug release, catalysis, photochemistry, electrochemistry, and functional polymers.<sup>[137,138]</sup>

Molecular modelling computational approaches, such as DFT and classical MD, are especially important to understand the structure and molecular processes involving these materials, since for most synthetic LDHs the crystal structure is very difficult to obtain due to their reduced crystallinity.<sup>[139]</sup> In order to lower the computational cost of the calculations, the first DFT models for the simulation of LDHs relied on anhydrous supercells<sup>[140]</sup> or cluster models.<sup>[141]</sup> The first realistic periodic models of LDHs suitable for DFT calculations were reported by Costa, Leitão, and their team.<sup>[142–144]</sup> Their models were adapted by Galvão et al. to obtain the  $[\text{Zn}_2\text{Al}(\text{OH})_6](\text{NO}_3)\cdot 2\text{H}_2\text{O}$  supercell shown in **Figure 8** for utilization with plane-wave DFT codes that consider the periodic cell approach.<sup>[145]</sup> At the time, there was still some uncertainty regarding the parallel<sup>[146,147]</sup> versus tilted<sup>[144,148]</sup> orientation of the nitrate anions inside LDH galleries, with DFT results supporting the tilted orientation.<sup>[145]</sup>

The models, together with periodic DFT calculations, were used to understand at the molecular and energetic level the morphological (SEM and AFM) and structural (XRD) results obtained for different forms of LDHs: i) Particles; ii) exfoliated single layer nanosheets, and iii) protective conversion films grown on top of aluminum alloys.<sup>[149]</sup> Fully formed LDH particles have a plate-like shape, whose lateral size is larger than the particle height.

Computed surface energies show that particles grow larger in length than in height to minimize their surface energy, since the lateral side of the particles is less stable than the top and bottom of the plates. Another conclusion drawn from the DFT calculations was that interaction energies are more favorable when LDHs interact side-by-side than when cationic layers and interlayers are stacked alternately, thus explaining why LDHs have larger widths than heights.<sup>[149]</sup> These results have subsequently been used to interpret the morphology of LDH particles by other authors.<sup>[150–154]</sup>

DFT calculations employing periodic models were also used to understand why formamide is the solvent of choice to promote the exfoliation of LDH particles to form single layer nanosheets.<sup>[155–159]</sup> It was revealed that, as formamide molecules substitute water molecules in the interlayer during the exfoliation treatment, the distance between cationic layers increases while the layer separation energy decreases.<sup>[149]</sup> As for LDH conversion films grown on top of aluminum alloys, there is a preference for LDH plates to grow perpendicularly to the surface, rather than lying flat on top of the aluminum surface and growing by stacking cationic layers separated by interlayers.<sup>[160–162]</sup> The conversion films were approximated in the DFT calculation as LDH clusters with different orientations and sizes on top of the surface. For both aluminum surfaces considered (Al(111) and  $\alpha\text{-Al}_2\text{O}_3$  (0001)), it was found that the most favorable interaction was with the cationic layers perpendicular to the aluminum surfaces, thus allowing to understand the SEM and AFM results obtained for these systems and explain the crystallization mechanism of LDH conversion films.<sup>[149]</sup>

DFT can be used to explore the relation between structure and energetics with high accuracy for relatively small LDH models (typically, less than 100 atoms). However, the time-dependent dynamics of larger and more realistic LDH systems with several thousands of atoms are better explored by classical MD, since it is less computationally expensive than DFT. For this reason, classical MD has been the traditional approach for the simulation of LDHs and other clay based materials,<sup>[163–165]</sup> with several reports in literature on the LDH structure.<sup>[166–170]</sup> Conversely, to successfully simulate the LDH stacked structure while maintaining the integrity of the cationic layers throughout the simulation, it is necessary to find the most appropriate MD procedure in terms of supercell model, force field parametrization and number of MD steps. Since there was a lack in literature of a straightforward recipe to perform MD simulations for these systems, Pérez-Sánchez et al.<sup>[171]</sup> developed an easy to follow MD framework using the GROMACS open source software, which can be tailored for a wide range of inorganic and organic anions intercalated in Mg(2)Al and Zn(2)Al LDHs. The well-defined simulation procedure can cope with long timescales (>100 ns) with all atomic positions allowed to move freely, while maintaining the integrity of the LDH structure intact. It was tested for different metals in the cationic layer (e.g., Mg(2)Al or Zn(2)Al combinations) and different intercalated anions (chloride, nitrate, and carbonate). It was also successfully tested for LDH particles in a sodium chloride water solution in terms of the stability of the cationic layers, and is now being extended for long-term anion exchange studies,<sup>[172]</sup> which, to the best of our knowledge, none of the previous computational models was able to do.<sup>[173,174]</sup> All the necessary parameters and inputs to carry out

the MD simulations are available online.<sup>[175]</sup> This MD procedure has already been employed by other researchers to understand the structure and processes involving LDHs for different applications,<sup>[136,176–178]</sup> and was employed in our research group, together with in-house tools,<sup>[179]</sup> to unveil the acid-base equilibrium, conformation and degree of solvation inside the interlayer galleries of an LDH material intercalating a well-known corrosion inhibitor, 2-mercaptobenzothiazole (MBT).<sup>[180]</sup> LDH-MBT is a nanostructured coating additive<sup>[181]</sup> and it was demonstrated that MD simulations can provide insights into the structural characterization performed by powder X-ray diffraction and the processes behind the weight loss indicated by thermogravimetric analysis.<sup>[182]</sup>

### 3.5. Metallic Surfaces

Corrosion inhibitors suppress or at least mitigate the corrosion degradation of metals, thus finding application in a wide range of industries and sectors. MBT is one of the most efficient and versatile organic corrosion inhibitors and was examined in depth by DFT calculations concerning its conformational, tautomeric, acid-base, non-covalent association, and ion-pair formation equilibrium,<sup>[180]</sup> as well as its adsorption mechanism onto periodic slab models of bare aluminum and aluminum oxide surfaces.<sup>[181]</sup> DFT was also employed to understand the trends observed in electrochemical studies for two triazole isomers tested for the protection of copper upon the calculation of structural and energetic details of the formation of protective films of both isomers onto a Cu(111) surface.<sup>[183]</sup>

Our research group is currently developing two complementary technological approaches to help corrosion scientists and engineers working in academia and across different industries to choose the optimal inhibitor for each specific corrosion problem: an interactive exploratory data tool and a machine learning-based application to design potential corrosion inhibitors.<sup>[184]</sup> Recently, an open data management web application to select corrosion inhibitors was developed.<sup>[185]</sup> The large and growing amount of corrosion inhibition efficiencies in literature required an efficient way to organize, access and compare the data. Nearly five thousand corrosion inhibition efficiencies and almost four hundred compounds have already been added to the database. The data originate from more than one hundred and twenty publications, for aluminum, copper, magnesium, iron, and their main alloys. The CORDATA application<sup>[186]</sup> can help corrosion scientists select appropriate corrosion inhibitors for applications with specific requirements.

The development of high throughput corrosion tests to evaluate the performance of corrosion inhibitors led to the availability of larger datasets, ideal for the application of ML and data-driven approaches.<sup>[8,83,187–193]</sup> The first works considered a few dozen inhibitors for aluminum alloys,<sup>[190–193]</sup> using a combination of ML algorithms and different types of molecular features, with promising results. One notable example was the use of ML to model one hundred corrosion inhibitors,<sup>[188]</sup> which produced the first robust models and concluded that more computationally expensive quantum chemistry descriptors are not required to obtain higher predictive performance from the models.<sup>[83,188,190]</sup> In other studies, it was also concluded that individual molecu-

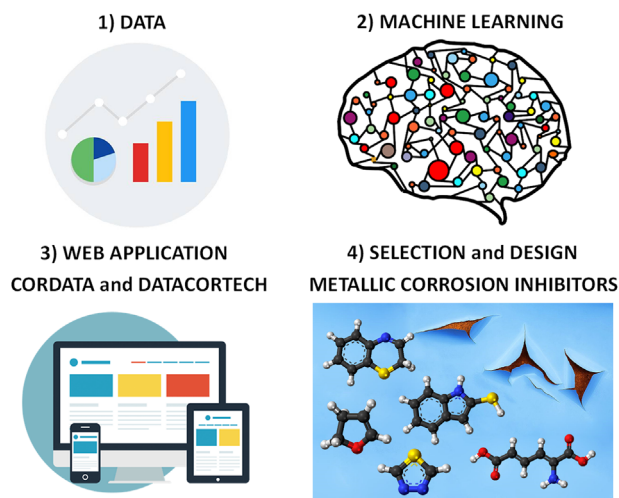


**Figure 9.** Data-driven technological approach used to select and design corrosion inhibitors for the protection of metallic surfaces.

lar features alone do not correlate with corrosion inhibition efficiencies, but that the use of ML is able to consider the interdependence of different features to predict corrosion inhibition efficiencies.<sup>[8,194,195]</sup> These works also motivated the use of ML to predict the controlled dissolution of magnesium alloys using organic compounds for the application in automotive, biomedical and energetic applications.<sup>[196–200]</sup>

The ML developments mentioned above considered data from a single or a restricted number of literature references. However, to increase the amount of data and diversify the chemical space available for ML, it is necessary to include data from different authors, laboratories and measured under different conditions, leading to so-called composite models. In a previous work, we tested the composite model approach considering inhibitor efficiencies for different types of aluminum alloys and pH values within the same model.<sup>[83]</sup> This increased the size of the dataset fourfold, thus resulting in an improved predictive performance due to an information gain. As a result, it has served as the basis of DATACORTECH,<sup>[201]</sup> an artificial intelligence application currently being developed for the virtual screening of potential corrosion inhibitors for the protection of aluminum alloys under different conditions.

The CORDATA and DATACORTECH applications represent an effort to digitalize and expedite the search for inhibitors, using the approach presented in **Figure 9**, to produce more robust and condition-specific corrosion-protective technologies.

### 3.6. MXenes

MXenes are two-dimensional materials which were first synthesized just over 10 years ago.<sup>[202,203]</sup> At the atomic level, their structure consists of very few layers of atoms of transition metal elements (M), intercalated with layers of carbon, nitrogen, or a mixture of the two (X). Traditionally, all MXene atomic layers have the same number of atoms, the outer layers being of the M element. The simplest MXenes have stoichiometry  $M_2X$ , with two M outer layers enclosing an X layer, and the atomic layers are stacked in a face-centered cubic (ABC) fashion. However,

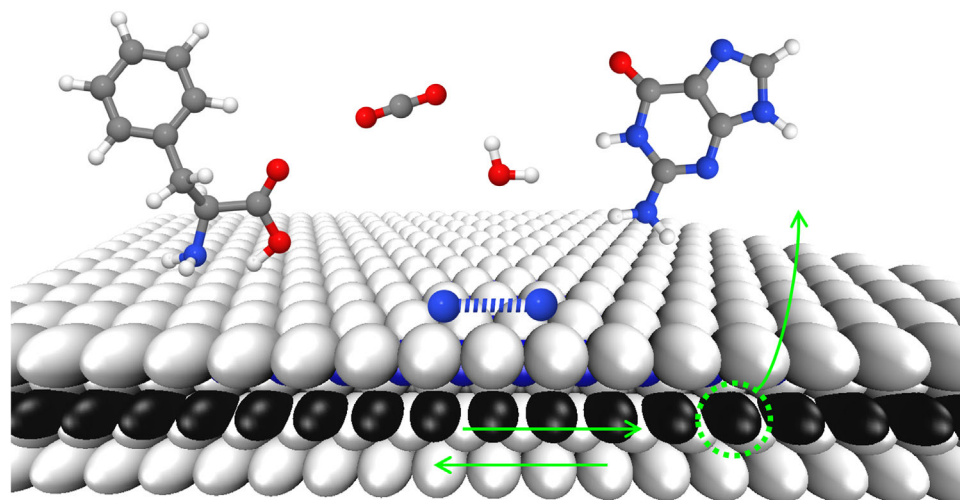


**Figure 10.** Illustration of several processes that have been studied on MXenes, namely molecule adsorption and dissociation, sliding of atomic layers, and creation of vacancies.

MXenes have been synthesized with more atomic layers, such as  $\text{Ti}_3\text{C}_2$ ,<sup>[203]</sup> with incomplete metallic layers, such as  $\text{Mo}_{1.33}\text{C}$ ,<sup>[204]</sup> with X layers made up of different elements, such as  $\text{Ti}_3\text{CN}$ ,<sup>[205]</sup> with M layers made up of different metals, such as  $\text{Mo}_2\text{TiC}_2$ ,<sup>[206]</sup> with a mixture of more than one metallic element on each M layer, such as  $\text{Ti}_{2-\gamma}\text{V}_\gamma\text{C}$ ,<sup>[207]</sup> or with their atomic layers stacked in a hexagonal close packed (ABA) manner, such as  $\text{Mo}_2\text{N}$ .<sup>[208]</sup> Furthermore, depending on the method for their synthesis and the surrounding environment, MXenes often present themselves covered by an external surface termination layer, usually composed of O, OH, H, F, or Cl groups.

The endless possible combinations of MXene stoichiometry, intra and interlayer atomic arrangement, and surface termination, theoretically allow one to tune their properties at will and confer MXenes a huge variety of applications. Generally, MXenes have high electrical conductivities, are hydrophilic, display very large surface areas, and can survive harsh conditions and highly corrosive environments, such as temperatures of nearly 1000 °C and pressures of tens of GPa.<sup>[209–211]</sup> This allows them to be applied in areas such as eco-friendly energy, water purification or catalysis.<sup>[212–214]</sup> We began studying these materials, mainly using DFT-based methods, in 2019, in very close collaboration with the group of Prof. Francesc Illas of the University of Barcelona, Spain, as a continuation of previous studies devoted to catalysis by metallic surfaces.<sup>[215–220]</sup> These works began with a theoretical analysis of the potential of MXenes to sense the presence of amino acids, and then quickly expanded to include the application of MXenes as catalysts, as well as to unveil more fundamental properties of MXenes, such as the way their atomic layers are stacked, or the energy required to create point defects on these surfaces (**Figure 10**).

MXenes with oxygen surface termination are excellent as sensors, since the termination layer acts as a shield that prevents molecules from adsorbing too strongly by bonding directly to the metallic layers of the material. One such example is the  $\text{Ti}_2\text{CO}_2$  MXene, which is made of titanium, the most biocompatible metal, and is therefore expected to be a suitable biosensor. By employing DFT-based calculations, we showed that this MX-

ene does indeed adsorb amino acids<sup>[221]</sup> and nucleobases<sup>[222]</sup> with moderate strength, as desired for sensing applications. While all nucleobases adsorb horizontally, that is, with their aromatic rings parallel to the MXene surface, some amino acids can form a chemical bond with a Ti atom, through the oxygen layer. We additionally found that the adsorption energies of the studied molecules correlate well with their van der Waals volumes, which allowed us to predict the strength of the interaction between the  $\text{Ti}_2\text{CO}_2$  MXene with other molecules, without performing additional calculations.

In the absence of surface termination, MXenes are substantially more reactive. They adsorb molecules much more strongly, activating them, and effectively work as catalysts. We used this fact to computationally study the adsorption and dissociation of water,<sup>[223]</sup> nitrogen,<sup>[224]</sup> and carbon dioxide<sup>[225]</sup> molecules on MXene surfaces, the latter having received experimental evidence.<sup>[226]</sup> We found that, in many cases, the reaction occurs almost spontaneously, that is, with no activation energy required. These results, obtained by a combination of DFT and microkinetic calculations, have gathered considerable interest from the scientific community because of their relevance to the industrial production of ammonia, for the hydrogen economy, and for large-scale carbon conversion, respectively, thus addressing key environmental issues and boosting the rapidly growing field of using MXenes in catalysis. During these studies, we noticed that some surfaces would undergo considerable distortion upon nitrogen adsorption, as if the atomic structure was attempting to change to another configuration. This motivated our fruitful search for alternative MXene structures. Indeed, we showed that many MXenes prefer to display a hexagonal close packed (ABA) stacking of their atomic layers, rather than the traditional face-centered cubic (ABC) one. This included not only the experimentally observed  $\text{Mo}_2\text{N}$ ,<sup>[208]</sup> and  $\text{Mo}_2\text{C}$ ,<sup>[212]</sup> but also many others, such as  $\text{W}_2\text{N}$ , the most efficient MXene to catalyze nitrogen dissociation,<sup>[224]</sup> which reduces the amount of energy required to break the molecule by around 98%.

MXenes have been used as catalysts, for instance for realizing the water-gas shift (WGS) reaction, which is crucial for the



industrial production of hydrogen.<sup>[212]</sup> MXenes completely devoid of surface termination cannot be used as catalysts on their own, since they are extremely reactive, and it is difficult to detach the products of reactions from the surface without damaging the MXene. On the other hand, MXenes with their surface completely terminated, for instance by oxygen, are too inactive and do not activate adsorbates. Therefore, for their successful application as catalysts, there must be a balance between patches of surface with and without surface termination,<sup>[227]</sup> or even between different surface terminations.<sup>[212]</sup> Our most recent studies have been oriented toward more realistic MXene models, starting by considering the formation of vacancy defects in MXenes.<sup>[228]</sup> These defects have been observed experimentally, an example being Mo–O double vacancies in the Mo<sub>2</sub>TiC<sub>2</sub> MXene,<sup>[227]</sup> and can contribute to the presence of neighboring surface patches with different surface termination. We additionally found that the latter is crucial for conducting the WGS reaction on the Mo<sub>2</sub>CT<sub>x</sub> MXene.<sup>[229]</sup> We considered different possibilities for the MXene surface termination, (T<sub>x</sub> = none, O, F, or a mixture of O and F) all plausible to be found upon synthesis, and concluded that its ideal composition should contain both F and O adatoms, which is precisely the experimentally observed composition.<sup>[212]</sup> In fact, Mo<sub>2</sub>CO<sub>2</sub> is too inert toward water adsorption and dissociation, while the Mo<sub>2</sub>CF<sub>2</sub> surface is damaged (removal of F terminations) after the reaction occurs, hence undesired for catalytic applications. In contrast, the bare Mo<sub>2</sub>C MXene would be a good candidate, but easily becomes irreversibly covered by O, because of the well-known oxophilicity of bare MXenes. The regions near one or two O adatoms among the F surface termination should provide all the advantages of each aforementioned surface termination, while avoiding their drawbacks. In fact, a combination of all three surface terminations allows exothermic water adsorption and its easy dissociation, comparable to those on bare MXenes, while the surface termination controls the exothermicity of the reaction and keeps the MXene from becoming saturated with O.<sup>[229]</sup>

Recently, we studied the possibility of epitaxially synthesizing MXenes, by taking advantage of the easy nitrogen dissociation that occurs on the surface of these materials.<sup>[230]</sup> The calculations show that the formation of fully N-covered M<sub>2</sub>XN<sub>2</sub> is kinetically possible for some M<sub>2</sub>X surfaces. Also, additional early transition metal adlayers are thermodynamically attainable, which can lead to M'<sub>2</sub>M<sub>2</sub>XN<sub>2</sub> MXenes.

#### 4. Final Remarks

At the Aveiro Institute of Materials, CICECO, we have been using several computational strategies, from quantum to classical mechanics approaches, from atomistic to coarse-grained models, to analyze the structures and properties of different classes of materials with potential applications in water remediation, gas adsorption/separation or catalysis. Additionally, we have been developing new tools to predict metal corrosion and to select the materials and conditions that can be used to prevent corrosion, to aid in the analysis of calculated data, and to facilitate the construction of molecular models and sets of parameters to run the simulations.

The studies we have been involved in over the past years have contributed with fundamental knowledge, on a molecular level,

on the mechanisms driving the adsorption of small gases in porous materials, such as MOFs, PMOs or titanosilicates. Currently, we are using computational tools to design MOFs with different structures and functionalizations in order to predict their potential for gas adsorption/separation, so the laborious and expensive experimental studies (synthesis, characterization, and testing) are performed only for the most promising materials, and will continue to contribute and promote discussion in this ever-growing research community.

Computer simulations of the adsorption of organic compounds on metal surfaces provided important information for the understanding of the formation of metal corrosion protective layers. The large library of adsorption energies is now being used to develop improved versions of machine learning algorithms that are promising for selecting the most appropriate corrosion inhibitor for a particular metal surface under specific conditions. Concurrently, ab initio and classical molecular dynamics are being used to understand the release of functional molecules from nanocontainers like LDHs when triggered by external stimuli such as pH change.

Despite having joined the large worldwide community of MXene research only three years ago, our group has covered different applications of MXenes, conducted several studies on their fundamental properties, motivated some experimental results and aided in explaining others. Presently, we are analyzing the effect of having transition metal atoms adsorbed on MXene surfaces on their catalytic activity and the mechanisms of important catalytic reactions, for example, WGS, on the surface of MXenes with patches of bare surface amid the usual terminations in this class of materials.

#### Acknowledgements

This work was developed within the scope of the projects CICECO - Aveiro Institute of Materials (UIDB/50011/2020, UIDP/50011/2020 and LA/P/0006/2020) and CERENA (UIDB/04028/2020 and UIDP/04028/2020), financed by national funds through the FCT/MEC (PIDDAC). It was also financed in the frame of projects SELMA (PTDC/REQ-QFI/4719/2014), SILVIA (PTDC/QUI-QFI/31002/2017 and CENTRO-01-0145-FEDER-31002), DataCor (POCI-01-0145-FEDER-030256 and PTDC/QUI-QFI/30256/2017, <https://datacorproject.wixsite.com/datacor>) and the European Union's Horizon 2020 research and innovation programme under the Marie Skłodowska-Curie grant agreement ID 101007430 (COAT4LIFE). The authors are also thankful to FCT I.P. for the computational resources granted in the framework of the Call for Advanced Computing Projects. G.P.-S. acknowledges the funding from FCT, I.P. (Decree-Laws 57/2016 and 2017). M.B. and B.Z. thank FCT for the Ph.D. grants SFRH/BD/147239/2019 and SFRH/BD/137751/2018, respectively. The authors acknowledge support from COST Action 18234 "Computational materials sciences for efficient water splitting with nanocrystals from abundant elements."

#### Conflict of Interest

The authors declare no conflict of interest.

#### Keywords

corrosion protection, density functional theory, gas adsorption/separation, heterogeneous catalysis, machine learning, molecular dynamics

Received: August 30, 2022  
Revised: November 2, 2022  
Published online:

- [1] T. J. Barton, L. M. Bull, W. G. Klemperer, D. A. Loy, B. McEnaney, M. Misono, P. A. Monson, G. Pez, G. W. Scherer, J. C. Vartuli, O. M. Yaghi, *Chem. Mater.* **1999**, *11*, 2633.
- [2] Global Markets for Inorganic Microporous and Nanoporous Adsorbents, <https://www.bccresearch.com/market-research/chemicals/inorganic-microporous-nanoporous-adsorbents.html> (accessed: August 2022).
- [3] P. Wollmann, M. Leistner, U. Stoeck, R. Grünker, K. Gedrich, N. Klein, O. Throl, W. Grähler, I. Senkovska, F. Dreisbach, S. Kaskel, *Chem. Commun.* **2011**, *47*, 5151.
- [4] B. Hammer, Y. Morikawa, J. K. Nørskov, *Phys. Rev. Lett.* **1996**, *76*, 2141.
- [5] J. R. B. Gomes, J. A. N. F. Gomes, *J. Mol. Struct.* **1999**, *463*, 163.
- [6] L. Mafra, T. Čendak, S. Schneider, P. V. Wiper, J. Pires, J. R. B. Gomes, M. L. Pinto, *J. Am. Chem. Soc.* **2017**, *139*, 389.
- [7] J. Schmidt, M. R. G. Marques, S. Botti, M. A. L. Marques, *npj Comput. Mater.* **2019**, *5*, 83.
- [8] A. Kokalj, M. Lozinšek, B. Kapun, P. Taheri, S. Neupane, P. Losada-Pérez, C. Xie, S. Stavber, D. Crespo, F. U. Renner, A. Mol, I. Milošev, *Corros. Sci.* **2021**, *179*, 108856.
- [9] J. M. Findley, D. S. Sholl, *J. Phys. Chem. C* **2021**, *125*, 24630.
- [10] A. Jain, S. P. Ong, G. Hautier, W. Chen, W. D. Richards, S. Dacek, S. Cholia, D. Gunter, D. Skinner, G. Ceder, K. A. Persson, *APL Mater.* **2013**, *1*, 011002.
- [11] C. Draxl, M. Scheffler, *J. Phys. Mater.* **2019**, *2*, 036001.
- [12] Y. Yan, Z. Shi, H. Li, L. Li, X. Yang, S. Li, H. Liang, Z. Qiao, *Chem. Eng. J.* **2022**, *427*, 131604.
- [13] A. Mazheika, Y.-G. Wang, R. Valero, F. Viñes, F. Illas, L. M. Ghiringhelli, S. V. Levchenko, M. Scheffler, *Nat. Commun.* **2022**, *13*, 419.
- [14] R. LeSar, *Introduction to Computational Materials Science*, Cambridge University Press, Cambridge, UK **2013**.
- [15] J. G. Lee, *Computational Materials Science*, CRC Press, Boca Raton, USA **2016**.
- [16] K. Ohno, K. Esfarjani, Y. Kawazoe, *Computational Materials Science*, Springer Berlin Heidelberg, Berlin, Heidelberg **2018**.
- [17] Nobel Prize Outreach AB 2022, The Nobel Prize in Chemistry 1998 press release, <https://www.nobelprize.org/prizes/chemistry/1998/press-release/> (accessed: August 2022).
- [18] P. Hohenberg, W. Kohn, *Phys. Rev.* **1964**, *136*, B864.
- [19] W. Kohn, L. J. Sham, *Phys. Rev.* **1965**, *140*, A1133.
- [20] J. P. Perdew, K. Schmidt, *AIP Conf. Proc.* **2001**, *577*, 1.
- [21] J. P. P. Ramalho, J. R. B. Gomes, F. Illas, *RSC Adv.* **2013**, *3*, 13085.
- [22] S. Grimme, A. Hansen, J. G. Brandenburg, C. Bannwarth, *Chem. Rev.* **2016**, *116*, 5105.
- [23] D. R. Bowler, T. Miyazaki, *Rep. Prog. Phys.* **2012**, *75*, 036503.
- [24] M. Levitt, A. Warshel, *Nature* **1975**, *253*, 694.
- [25] R. Hills, C. Brooks, *Int. J. Mol. Sci.* **2009**, *10*, 889.
- [26] K. Binder, A. Milchev, *J. Comput.-Aided Mater. Des.* **2002**, *9*, 33.
- [27] O. Kletnik-Edelman, C. G. Sztrum-Vartash, E. Rabani, *J. Mater. Chem.* **2009**, *19*, 2872.
- [28] R. G. Larson, L. E. Scriven, H. T. Davis, *J. Chem. Phys.* **1985**, *83*, 2411.
- [29] R. G. Larson, *J. Chem. Phys.* **1988**, *89*, 1642.
- [30] L. Sarkisov, P. A. Monson, *Phys. Rev. E* **2001**, *65*, 011202.
- [31] A. Patti, A. D. Mackie, F. R. Siperstein, *Langmuir* **2007**, *23*, 6771.
- [32] F. R. Siperstein, K. E. Gubbins, *Langmuir* **2003**, *19*, 2049.
- [33] S. M. Auerbach, M. H. Ford, P. A. Monson, *Curr. Opin. Colloid Interface Sci.* **2005**, *10*, 220.
- [34] S. J. Marrink, H. J. Risselada, S. Yefimov, D. P. Tieleman, A. H. de Vries, *J. Phys. Chem. B* **2007**, *111*, 7812.
- [35] S. J. Marrink, L. Monticelli, M. N. Melo, R. Alessandri, D. P. Tieleman, P. C. T. Souza, *Wiley Interdiscip. Rev.: Comput. Mol. Sci.* **2022**, e1620, <https://doi.org/10.1002/wcms.1620>.
- [36] S. J. Marrink, D. P. Tieleman, *Chem. Soc. Rev.* **2013**, *42*, 6801.
- [37] G. Pérez-Sánchez, J. R. B. Gomes, M. Jorge, *Langmuir* **2013**, *29*, 2387.
- [38] G. Pérez-Sánchez, S.-C. Chien, J. R. B. Gomes, M. N. D. S. Cordeiro, S. M. Auerbach, P. A. Monson, M. Jorge, *Chem. Mater.* **2016**, *28*, 2715.
- [39] M. Jorge, A. W. Milne, O. N. Sobek, A. Centi, G. Pérez-Sánchez, J. R. B. Gomes, *Mol. Simul.* **2018**, *44*, 435.
- [40] R. Alessandri, F. Grünewald, S. J. Marrink, *Adv. Mater.* **2021**, *33*, 2008635.
- [41] L. Monticelli, S. K. Kandasamy, X. Periole, R. G. Larson, D. P. Tieleman, S.-J. Marrink, *J. Chem. Theory Comput.* **2008**, *4*, 819.
- [42] S. Y. Joshi, S. A. Deshmukh, *Mol. Simul.* **2021**, *47*, 786.
- [43] P. C. T. Souza, R. Alessandri, J. Barnoud, S. Thallmair, I. Faustino, F. Grünewald, I. Patmanidis, H. Abdizadeh, B. M. H. Bruininks, T. A. Wassenaar, P. C. Kroon, J. Melcr, V. Nieto, V. Corradi, H. M. Khan, J. Domański, M. Javanainen, H. Martinez-Seara, N. Reuter, R. B. Best, I. Vattulainen, L. Monticelli, X. Periole, D. P. Tieleman, A. H. de Vries, S. J. Marrink, *Nat. Methods* **2021**, *18*, 382.
- [44] W. D. C. Moebis, *Math. Biosci.* **1974**, *22*, 113.
- [45] D. T. Gillespie, *J. Comput. Phys.* **1976**, *22*, 403.
- [46] A. P. J. Jansen, *Comput. Phys. Commun.* **1995**, *86*, 1.
- [47] A. Rahbari, R. Hens, M. Ramdin, O. A. Moultois, D. Dubbeldam, T. J. H. Vlugt, *Mol. Simul.* **2021**, *47*, 804.
- [48] M. Andersen, C. Panosetti, K. Reuter, *Front Chem* **2019**, *7*, 202.
- [49] Z. Jing, L. Xin, H. Sun, *Phys. Chem. Chem. Phys.* **2015**, *17*, 25421.
- [50] A. C. T. van Duin, S. Dasgupta, F. Lorant, W. A. Goddard, *J. Phys. Chem. A* **2001**, *105*, 9396.
- [51] T. Du, H. Li, G. Sant, M. Bauchy, *J. Chem. Phys.* **2018**, *148*, 234504.
- [52] S. Urata, A.-T. Kuo, H. Murofushi, *Phys. Chem. Chem. Phys.* **2021**, *23*, 14486.
- [53] S. Yang, J. Qu, *Polymer* **2012**, *53*, 4806.
- [54] H. B. Fan, M. M. F. Yuen, *Polymer* **2007**, *48*, 2174.
- [55] S. Yu, S. Yang, M. Cho, *Polymer* **2009**, *50*, 945.
- [56] M. Kotelyanskii, N. J. Wagner, M. E. Paulaitis, *Macromolecules* **1996**, *29*, 8497.
- [57] N. J. Soni, P.-H. Lin, R. Khare, *Polymer* **2012**, *53*, 1015.
- [58] L. Jin, S. M. Auerbach, P. A. Monson, *Langmuir* **2013**, *29*, 766.
- [59] A. P. Carvalho, S. M. Santos, G. Pérez-Sánchez, J. D. Gouveia, J. R. B. Gomes, M. Jorge, *npj Comput. Mater.* **2022**, *8*, 49.
- [60] J. Krajniak, Z. Zhang, S. Pandiyan, E. Nies, G. Samaey, *J. Comput. Chem.* **2018**, *39*, 1764.
- [61] G. E. Norman, V. S. Filinov, *High Temp.* **1969**, *7*, 216.
- [62] N. Metropolis, A. W. Rosenbluth, M. N. Rosenbluth, A. H. Teller, E. Teller, *J. Chem. Phys.* **1953**, *21*, 1087.
- [63] S. Caro-Ortiz, E. Zuidema, D. Dekker, M. Rigutto, D. Dubbeldam, T. J. H. Vlugt, *J. Phys. Chem. C* **2020**, *124*, 21782.
- [64] A. R. Kulkarni, D. S. Sholl, *J. Phys. Chem. C* **2016**, *120*, 23044.
- [65] M. Jorge, M. Fischer, J. R. B. Gomes, C. Siquet, J. C. Santos, A. E. Rodrigues, *Ind. Eng. Chem. Res.* **2014**, *53*, 15475.
- [66] C. Campbell, C. A. Ferreiro-Rangel, M. Fischer, J. R. B. Gomes, M. Jorge, *J. Phys. Chem. C* **2017**, *121*, 441.
- [67] C. Campbell, J. R. B. Gomes, M. Fischer, M. Jorge, *J. Phys. Chem. Lett.* **2018**, *9*, 3544.
- [68] J. I. Siepmann, D. Frenkel, *Mol. Phys.* **1992**, *75*, 59.
- [69] N. H. Phan, S. Rio, C. Faur, L. L. Coq, P. L. Cloirec, T. H. Nguyen, *Carbon* **2006**, *44*, 2569.
- [70] S. J. Allen, L. Whitten, G. McKay, *Dev. Chem. Eng. Miner. Process.* **2008**, *6*, 231.

- [71] J.-C. Liu, P. A. Monson, *Ind. Eng. Chem. Res.* **2006**, *45*, 5649.
- [72] E. Di Biase, L. Sarkisov, *Carbon* **2013**, *64*, 262.
- [73] A. Gonciaruk, F. R. Siperstein, *Carbon* **2015**, *88*, 185.
- [74] D. Bahamon, L. Carro, S. Guri, L. F. Vega, *J. Colloid Interface Sci.* **2017**, *498*, 323.
- [75] J. M. Pereira, V. Calisto, S. M. Santos, *J. Mol. Liq.* **2019**, *279*, 669.
- [76] J. M. Pereira, S. M. Santos, CarbGen Tool, <http://carbgen.web.ua.pt/> (accessed: August 2022).
- [77] J. M. Pereira, CarbGen.py, <https://github.com/JosePereiraUA/CarbGen.py> (accessed: August 2022).
- [78] J. M. Pereira, S. M. Santos, ProtoSyn.jl, <https://github.com/sergiosantos-group/ProtoSyn.jl> (accessed: August 2022).
- [79] A. Y. T. Wang, R. J. Murdock, S. K. Kauwe, A. O. Oliynyk, A. Gurlo, J. Brgoch, K. A. Persson, T. D. Sparks, *Chem. Mater.* **2020**, *32*, 4954.
- [80] S. M. Moosavi, K. M. Jablonka, B. Smit, *J. Am. Chem. Soc.* **2020**, *142*, 20273.
- [81] A. M. Molinaro, R. Simon, R. M. Pfeiffer, *Bioinformatics* **2005**, *21*, 3301.
- [82] N. R. Barraza, A. A. Moreno, in *Anales de las 49 JAAIO: XXI Simposio Argentino de Inteligencia Artificial* (Eds: M. Beiró, R. Wachenchauser, Y. B. Seibene), Buenos Aires, Argentina **2020**, pp. 15–27.
- [83] T. L. P. Galvão, G. Novell-Leruth, A. Kuznetsova, J. Tedim, J. R. B. Gomes, *J. Phys. Chem. C* **2020**, *124*, 5624.
- [84] R. Schwartz-Ziv, A. Armon, *Inf. Fusion* **2021**, *81*, 84.
- [85] G. Shmueli, *Stat. Sci.* **2011**, *25*, 289.
- [86] H. Furukawa, K. E. Cordova, M. O’Keeffe, O. M. Yaghi, *Science* **2013**, *341*, 974.
- [87] J. R. B. Gomes, J. L. C. Fajín, M. N. D. S. Cordeiro, C. Teixeira, P. Gomes, R. S. Pillai, G. Novell-Leruth, J. Toda, M. Jorge, in *Density Functional Theory: Principles, Applications and Analysis* (Eds: J. Morin, J. M. Pelletier), Nova Science Publishers, Inc., New York, USA **2013**, pp. 1–57.
- [88] A. Li, R. B. Perez, S. Wiggin, S. C. Ward, P. A. Wood, D. Fairen-Jimenez, *Matter* **2021**, *4*, 1105.
- [89] K. Adil, Y. Belmabkhout, R. S. Pillai, A. Cadiou, P. M. Bhatt, A. H. Assen, G. Maurin, M. Eddaoudi, *Chem. Soc. Rev.* **2017**, *46*, 3402.
- [90] C. A. Trickett, A. Helal, B. A. Al-Maythaly, Z. H. Yamani, K. E. Cordova, O. M. Yaghi, *Nat. Rev. Mater.* **2017**, *2*, 17045.
- [91] J. Liu, L. Chen, H. Cui, J. Zhang, L. Zhang, C. Y. Su, *Chem. Soc. Rev.* **2014**, *43*, 6011.
- [92] W. P. Lustig, S. Mukherjee, N. D. Rudd, A. V. Desai, J. Li, S. K. Ghosh, *Chem. Soc. Rev.* **2017**, *46*, 3242.
- [93] W. Xia, A. Mahmood, R. Zou, Q. Xu, *Energy Environ. Sci.* **2015**, *8*, 1837.
- [94] J. Li, X. Wang, G. Zhao, C. Chen, Z. Chai, A. Alsaedi, T. Hayat, X. Wang, *Chem. Soc. Rev.* **2018**, *47*, 2322.
- [95] M. Giménez-Marqués, T. Hidalgo, C. Serre, P. Horcajada, *Coord. Chem. Rev.* **2016**, *307*, 342.
- [96] A. Li, R. Bueno-Perez, D. Madden, D. Fairen-Jimenez, *Chem. Sci.* **2022**, *13*, 7990.
- [97] M. Fischer, J. R. B. Gomes, M. Fröba, M. Jorge, *Langmuir* **2012**, *28*, 8537.
- [98] M. Fischer, J. R. B. Gomes, M. Jorge, *Mol. Simul.* **2014**, *40*, 537.
- [99] R. S. Pillai, M. L. Pinto, J. Pires, M. Jorge, J. R. B. Gomes, *ACS Appl. Mater. Interfaces* **2015**, *7*, 624.
- [100] J. Pires, J. Fernandes, K. Dedeker, J. R. B. Gomes, G. Pérez-Sánchez, F. Nouar, C. Serre, M. L. Pinto, *ACS Appl. Mater. Interfaces* **2019**, *11*, 27410.
- [101] K. Sladekova, C. Campbell, C. Grant, A. J. Fletcher, J. R. B. Gomes, M. Jorge, *Adsorption* **2020**, *26*, 663.
- [102] S. M. F. Vilela, J. A. R. Navarro, P. Barbosa, R. F. Mendes, G. Pérez-Sánchez, H. Nowell, D. Ananias, F. Figueiredo, J. R. B. Gomes, J. P. C. Tomé, F. A. A. Paz, *J. Am. Chem. Soc.* **2021**, *143*, 1365.
- [103] Y. Wang, S. B. Peh, D. Zhao, *Small* **2019**, *15*, e1900058.
- [104] K. Momma, F. Izumi, *J. Appl. Crystallogr.* **2011**, *44*, 1272.
- [105] J. Pires, M. L. Pinto, V. K. Saini, *ACS Appl. Mater. Interfaces* **2014**, *6*, 12093.
- [106] T. Asefa, M. J. MacLachlan, N. Coombs, G. A. Ozin, *Nature* **1999**, *402*, 867.
- [107] S. Inagaki, S. Guan, Y. Fukushima, T. Ohsuna, O. Terasaki, *J. Am. Chem. Soc.* **1999**, *121*, 9611.
- [108] B. J. Melde, B. T. Holland, C. F. Blanford, A. Stein, *Chem. Mater.* **1999**, *11*, 3302.
- [109] P. Van der Voort, D. Esquivel, E. De Canck, F. Goethals, I. Van Driessche, F. J. Romero-Salguero, *Chem. Soc. Rev.* **2013**, *42*, 3913.
- [110] P. Ferreira, C. Bispo, M. A. O. Lourenço, J. R. B. Gomes, N. Bion, K. D. O. Vigier, F. Jérôme, in *Comprehensive Guide for Mesoporous Materials, Volume 4: Application and Commercialization* (Ed: M. Aliofk-hazraei), Nova Science Publishers, Inc., New York, USA **2015**, pp. 261–295.
- [111] M. A. O. Lourenço, J. R. B. Gomes, P. Ferreira, in *Hybrid Org. Interfaces Toward Adv. Funct. Mater.* (Eds: M.-H. Delville, A. Taubert), Wiley-VCH Verlag GmbH & Co. KGaA, Weinheim, Germany **2018**, pp. 413–458.
- [112] U. Martinez, G. Pacchioni, *Microporous Mesoporous Mater.* **2010**, *129*, 62.
- [113] M. A. O. Lourenço, C. Siquet, J. C. Santos, M. Jorge, J. R. B. Gomes, P. Ferreira, *J. Phys. Chem. C* **2016**, *120*, 14236.
- [114] M. A. O. Lourenço, C. Siquet, M. Sardo, J. Pires, L. Mafra, M. Jorge, M. L. Pinto, P. Ferreira, J. R. B. Gomes, *J. Phys. Chem. C* **2016**, *120*, 3863.
- [115] M. A. O. Lourenço, P. Ferreira, J. R. B. Gomes, *Mater. Today Commun.* **2021**, *26*, 102088.
- [116] M. A. O. Lourenço, P. Ferreira, J. R. B. Gomes, *Phys. Chem. Chem. Phys.* **2018**, *20*, 16686.
- [117] A. Comotti, S. Bracco, P. Valsesia, L. Ferretti, P. Sozzani, *J. Am. Chem. Soc.* **2007**, *129*, 8566.
- [118] G. N. Kalantzopoulos, M. K. Antoniou, A. Enotiadis, K. Dimos, E. Maccallini, A. Policicchio, E. Colavita, R. G. Agostino, *J. Mater. Chem. A* **2016**, *4*, 9275.
- [119] S. L. Suib, *Chem. Rec.* **2017**, *17*, 1169.
- [120] C. T. Kresge, W. J. Roth, *Chem. Soc. Rev.* **2013**, *42*, 3663.
- [121] A. Monnier, F. Schüth, Q. Huo, D. Kumar, D. Margolese, R. S. Maxwell, G. D. Stucky, M. Krishnamurty, P. Petroff, A. Firouzi, M. Janicke, B. F. Chmelka, *Science* **1993**, *261*, 1299.
- [122] M. Jorge, J. R. B. Gomes, M. N. D. S. Cordeiro, N. A. Seaton, *J. Am. Chem. Soc.* **2007**, *129*, 15414.
- [123] M. Jorge, J. R. B. Gomes, M. N. D. S. Cordeiro, N. A. Seaton, *J. Phys. Chem. B* **2009**, *113*, 708.
- [124] J. R. B. Gomes, M. N. D. S. Cordeiro, M. Jorge, *Geochim. Cosmochim. Acta* **2008**, *72*, 4421.
- [125] S.-C. Chien, G. Pérez-Sánchez, J. R. B. Gomes, M. N. D. S. Cordeiro, M. Jorge, S. M. Auerbach, P. A. Monson, *J. Phys. Chem. C* **2017**, *121*, 4564.
- [126] A. Firouzi, F. Atef, A. G. Oertli, G. D. Stucky, B. F. Chmelka, *J. Am. Chem. Soc.* **1997**, *119*, 3596.
- [127] P. T. Tanev, T. J. Pinnavaia, *Science* **1995**, *267*, 865.
- [128] A. Centi, M. Jorge, *Langmuir* **2016**, *32*, 7228.
- [129] A. Centi, J. R. H. Manning, V. Srivastava, S. van Meurs, S. V. Patwardhan, M. Jorge, *Mater. Horiz.* **2019**, *6*, 1027.
- [130] A. Carvalho, SILVIA project, <https://github.com/4ndrecarvalho/SILVIA> (accessed: August 2022).
- [131] F. Devreux, J. P. Boilot, F. Chaput, A. Lecomte, *Phys. Rev. A* **1990**, *41*, 6901.
- [132] A. Malani, S. M. Auerbach, P. A. Monson, *J. Phys. Chem. Lett.* **2010**, *1*, 3219.
- [133] X. Duan, D. G. Evans *Layered Double Hydroxides. Structure and Bonding vol. 119*, Springer-Verlag, Heidelberg, Germany **2006**.

- [134] J. Tedim, S. K. Poznyak, A. Kuznetsova, D. Raps, T. Hack, M. L. Zheludkevich, M. G. S. Ferreira, *ACS Appl. Mater. Interfaces* **2010**, *2*, 1528.
- [135] T. L. P. Galvão, M. Wilhelm, J. R. B. Gomes, J. Tedim, in *Micro and Nano Technologies, Smart Nanocontainers* (Eds: P. Nguyen-Tri, T.-O. Do, T. A. Nguyen), Elsevier, Amsterdam **2020**, p. 385.
- [136] S. Zhu, M. A. Khan, T. Kameda, H. Xu, F. Wang, M. Xia, T. Yoshioka, *J. Hazard. Mater.* **2022**, *426*, 128062.
- [137] R. Tian, R. Liang, M. Wei, D. G. Evans, X. Duan, in *50 Years of Structure and Bonding—The Anniversary Volume*, Vol. 172 (Ed: D. Mingos), Springer Cham, Switzerland **2016**, p. 65.
- [138] Q. Wang, D. O'Hare, *Chem. Rev.* **2012**, *112*, 4124.
- [139] G. S. Thomas, P. V. Kamath, *J. Chem. Sci.* **2006**, *118*, 127.
- [140] A. Trave, A. Selloni, A. Goursot, D. Tichit, J. Weber, *J. Phys. Chem. B* **2002**, *106*, 12291.
- [141] H. Yan, J. Lu, M. Wei, J. Ma, H. Li, J. He, D. G. Evans, X. Duan, *J. Mol. Struct.* **2008**, *866*, 34.
- [142] D. G. Costa, A. B. Rocha, W. F. Souza, S. S. X. Chiaro, A. A. Leitão, *J. Phys. Chem. C* **2008**, *112*, 10681.
- [143] D. G. Costa, A. B. Rocha, R. Diniz, W. F. Souza, S. S. X. Chiaro, A. A. Leitão, *J. Phys. Chem. C* **2010**, *114*, 14133.
- [144] D. G. Costa, A. B. Rocha, W. F. Souza, S. S. X. Chiaro, A. A. Leitão, *Appl. Clay Sci.* **2012**, *56*, 16.
- [145] T. L. P. Galvão, C. S. Neves, A. P. F. Caetano, F. Maia, D. Mata, E. Malheiro, M. J. Ferreira, A. C. Bastos, A. N. Salak, J. R. B. Gomes, J. Tedim, M. G. S. Ferreira, *J. Colloid Interface Sci.* **2016**, *468*, 86.
- [146] Q. Xu, Z. M. Ni, J. H. Mao, *J. Mol. Struct.* **2009**, *915*, 122.
- [147] Z. P. Xu, H. C. Zeng, *J. Phys. Chem. B* **2001**, *105*, 1743.
- [148] A. N. Salak, J. Tedim, A. I. Kuznetsova, J. L. Ribeiro, L. G. Vieira, M. L. Zheludkevich, M. G. S. Ferreira, *Chem. Phys.* **2012**, *397*, 102.
- [149] T. L. P. Galvão, C. S. Neves, M. L. Zheludkevich, J. R. B. Gomes, J. Tedim, M. G. S. Ferreira, *J. Phys. Chem. C* **2017**, *121*, 2211.
- [150] W. Li, A. Liu, H. Tian, D. Wang, *Colloid Interface Sci. Commun.* **2018**, *24*, 18.
- [151] L. Wu, B. Peng, Q. Li, Q. Wang, X. Yan, Q. Lin, C. Ji, *Environ. Sci. Pollut. Res.* **2019**, *26*, 19665.
- [152] G. Prestopino, G. Arrabito, A. Generosi, A. Mattochia, B. Paci, G. Perez, G. Verona-Rinati, P. G. Medaglia, *Sci. Rep.* **2019**, *9*, 11498.
- [153] D. K. Aleshin, M. A. Mashkovtsev, V. N. Rychkov, G. M. Bunkov, E. O. Baksheev, N. V. Zhirenkina, *Powder Technol.* **2020**, *376*, 12.
- [154] J. Roberts, Y. Song, M. Crocker, C. Risko, *J. Chem. Inf. Model.* **2020**, *60*, 4845.
- [155] F. Song, X. Hu, *Nat. Commun.* **2014**, *5*, 4477.
- [156] R. Ma, Z. Liu, L. Li, N. Iyi, T. Sasaki, *J. Mater. Chem.* **2006**, *16*, 3809.
- [157] Z. Liu, R. Ma, M. Osada, N. Iyi, Y. Ebin, K. Takada, T. Sasaki, *J. Am. Chem. Soc.* **2006**, *128*, 4872.
- [158] J. B. Han, J. Lu, M. Wei, Z. L. Wang, X. Duan, *Chem. Commun.* **2008**, *41*, 5188.
- [159] G. Abellán, E. Coronado, C. Martí-Gastaldo, E. Pinilla-Cienfuegos, A. Ribera, *J. Mater. Chem.* **2010**, *20*, 7451.
- [160] J. Tedim, M. L. Zheludkevich, A. N. Salak, A. Lisenkov, M. G. S. Ferreira, *J. Mater. Chem.* **2011**, *21*, 15464.
- [161] J. Tedim, M. L. Zheludkevich, A. C. Bastos, A. N. Salak, J. Carneiro, F. Maia, A. D. Lisenkov, A. B. Oliveira, M. G. S. Ferreira, *ECS Electrochem. Lett.* **2013**, *3*, C4.
- [162] J. Tedim, M. L. Zheludkevich, A. C. Bastos, A. N. Salak, A. D. Lisenkov, M. G. S. Ferreira, *Electrochim. Acta* **2014**, *117*, 164.
- [163] R. T. Cygan, J.-J. Liang, A. G. Kalinichev, *J. Phys. Chem. B* **2004**, *108*, 1255.
- [164] H. C. Greenwell, W. Jones, P. V. Coveney, S. Stackhouse, *J. Mater. Chem.* **2006**, *16*, 708.
- [165] R. T. Cygan, J. A. Greathouse, H. Heinz, A. G. Kalinichev, *J. Mater. Chem.* **2009**, *19*, 2470.
- [166] N. Kim, Y. Kim, T. T. Tsotsis, M. Sahimi, *J. Chem. Phys.* **2005**, *122*, 214713.
- [167] N. Kim, A. Harale, T. T. Tsotsis, M. Sahimi, *J. Chem. Phys.* **2007**, *127*, 224701.
- [168] P. Tran, S. Smith, H. Zhang, Z. P. Xu, Y. Wong, G. Q. Lu, *J. Phys. Chem. Solids* **2008**, *69*, 1044.
- [169] J. Pisson, J. P. Morel, N. Morel-Desrosiers, C. Taviot-Guého, P. Malreyt, *J. Phys. Chem. B* **2008**, *112*, 7856.
- [170] G. M. Lombardo, G. C. Pappalardo, F. Punzo, F. Costantino, U. Costantino, M. Sisani, *Eur. J. Inorg. Chem.* **2005**, *2005*, 5026.
- [171] G. Pérez-Sánchez, T. L. P. Galvão, J. Tedim, J. R. B. Gomes, *Appl. Clay Sci.* **2018**, *163*, 164.
- [172] G. Novell-Leruth, A. Kuznetsova, J. Tedim, J. R. B. Gomes, T. L. P. Galvão, *Nanomaterials* **2022**, *12*, 4039.
- [173] A. A. Tsukanov, S. G. Psakhie, *Sci. Rep.* **2016**, *6*, 19986.
- [174] F. A. Rad, Z. Rezvani, F. Khodam, *RSC Adv.* **2016**, *6*, 11193.
- [175] G. Pérez-Sánchez, T. L. P. Galvão, J. Tedim, J. R. B. Gomes, LDH models: Input files for MD simulations using Gromacs, <http://sweet.ua.pt/jrgomes/SELMA/MD-LDH/> (accessed: August 2022).
- [176] S. R. Tavares, J. F. S. Haddad, P. I. R. Moraes, A. A. Leitão, *Appl. Surf. Sci.* **2020**, *513*, 145743.
- [177] M. Pšenička, J. Škoda, M. Pospíšil, *Appl. Clay Sci.* **2020**, *189*, 105560.
- [178] X. Li, T. Würger, C. Feiler, R. H. Meißner, M. Serdechnova, C. Blawert, M. L. Zheludkevich, *ACS Omega* **2022**, *7*, 12412.
- [179] G. Novell-Leruth, LDH\_MBT\_codes, [https://github.com/gnovell/LDH\\_MBT\\_codes](https://github.com/gnovell/LDH_MBT_codes) (accessed: August 2022).
- [180] T. L. P. Galvão, A. Kuznetsova, J. R. B. Gomes, M. L. Zheludkevich, J. Tedim, M. G. S. Ferreira, *Theor. Chem. Acc.* **2016**, *135*, 78.
- [181] T. L. P. Galvão, I. Sousa, M. Wilhelm, J. Carneiro, J. Opršal, H. Kukačková, V. Špaček, F. Maia, J. R. B. Gomes, J. Tedim, M. G. S. Ferreira, *Chem. Eng. J.* **2018**, *341*, 526.
- [182] G. Novell-Leruth, G. Pérez-Sánchez, T. L. P. Galvão, D. Boiba, S. Poznyak, J. Carneiro, J. Tedim, J. R. B. Gomes, *Appl. Clay Sci.* **2020**, *198*, 105842.
- [183] S. U. Ofoegbu, T. L. P. Galvão, J. R. B. Gomes, J. Tedim, H. I. S. Nogueira, M. G. S. Ferreira, M. L. Zheludkevich, *Phys. Chem. Chem. Phys.* **2017**, *19*, 6113.
- [184] T. L. P. Galvão, G. Novell-Leruth, I. Ferreira, A. Kuznetsova, J. R. B. Gomes, J. Tedim, *Mater. Proc.* **2021**, *6*, 32.
- [185] T. L. P. Galvão, I. Ferreira, A. Kuznetsova, G. Novell-Leruth, C. Song, C. Feiler, S. V. Lamaka, C. Rocha, F. Maia, M. L. Zheludkevich, J. R. B. Gomes, J. Tedim, *npj Mater. Degrad.* **2022**, *6*, 48.
- [186] T. L. P. Galvão, CORDATA, <https://datacor.shinyapps.io/cordata/> (accessed: August 2021).
- [187] L. B. Coelho, D. Zhang, Y. Van Ingelgem, D. Steckelmacher, A. Nowé, H. Terry, *npj Mater. Degrad.* **2022**, *6*, 8.
- [188] D. A. Winkler, M. Breedon, P. White, A. E. Hughes, E. D. Sapper, I. Cole, *Corros. Sci.* **2016**, *106*, 229.
- [189] D. A. Winkler, *Metals* **2017**, *7*, 553.
- [190] D. A. Winkler, M. Breedon, A. E. Hughes, F. R. Burden, A. S. Barnard, T. G. Harvey, I. Cole, *Green Chem.* **2014**, *16*, 3349.
- [191] M. Breedon, M. C. Per, I. S. Cole, A. S. Barnard, *J. Mater. Chem. A* **2014**, *2*, 16660.
- [192] M. Fernandez, M. Breedon, I. S. Cole, A. S. Barnard, *Chemosphere* **2016**, *160*, 80.
- [193] F. F. Chen, M. Breedon, P. White, C. Chu, D. Mallick, S. Thomas, E. Sapper, I. Cole, *Mater. Des.* **2016**, *112*, 410.
- [194] A. Kokalj, C. Xie, I. Milošev, D. Crespo, *Corros. Sci.* **2021**, *193*, 109900.
- [195] A. Kokalj, *Corros. Sci.* **2021**, *193*, 109650.
- [196] T. Würger, C. Feiler, F. Musil, G. B. V. Feldbauer, D. Höche, S. V. Lamaka, M. L. Zheludkevich, R. H. Meißner, *Front. Mater.* **2019**, *6*, 53.
- [197] C. Feiler, D. Mei, B. Vaghefnazari, T. Würger, R. H. Meißner, B. J. C. Luthringer-Feyerabend, D. A. Winkler, M. L. Zheludkevich, S. V. Lamaka, *Corros. Sci.* **2020**, *163*, 108245.
- [198] C. Feiler, D. Mei, B. J. C. Luthringer-Feyerabend, S. V. Lamaka, M. L. Zheludkevich, *Corrosion* **2021**, *77*, 204.

- [199] T. Würger, D. Mei, B. Vaghefinazari, D. A. Winkler, S. V. Lamaka, M. L. Zheludkevich, R. H. Meißner, C. Feiler, *npj Mater. Degrad.* **2021**, 5, 2.
- [200] E. J. Schiessler, T. Würger, S. V. Lamaka, R. H. Meißner, C. J. Cyron, M. L. Zheludkevich, C. Feiler, R. C. Aydin, *npj Comput. Mater.* **2021**, 7, 193.
- [201] T. L. P. Galvão, DATACORTECH, <https://datacor.shinyapps.io/datacortech/> (accessed: August 2022).
- [202] M. Naguib, V. N. Mochalin, M. W. Barsoum, Y. Gogotsi, *Adv. Mater.* **2014**, 26, 992.
- [203] M. Naguib, M. Kurtoglu, V. Presser, J. Lu, J. Niu, M. Heon, L. Hultman, Y. Gogotsi, M. W. Barsoum, *Adv. Mater.* **2011**, 23, 4248.
- [204] I. Persson, A. el Ghazaly, Q. Tao, J. Halim, S. Kota, V. Darakchieva, J. Palisaitis, M. W. Barsoum, J. Rosen, P. O. Å. Persson, *Small* **2018**, 14, 1703676.
- [205] M. Naguib, O. Mashtalir, J. Carle, V. Presser, J. Lu, L. Hultman, Y. Gogotsi, M. W. Barsoum, *ACS Nano* **2012**, 6, 1322.
- [206] B. Anasori, Y. Xie, M. Beidaghi, J. Lu, B. C. Hosler, L. Hultman, P. R. C. Kent, Y. Gogotsi, M. W. Barsoum, *ACS Nano* **2015**, 9, 9507.
- [207] M. Han, K. Maleski, C. E. Shuck, Y. Yang, J. T. Glazar, A. C. Foucher, K. Hantanasirisakul, A. Sarycheva, N. C. Frey, S. J. May, V. B. Shenoy, E. A. Stach, Y. Gogotsi, *J. Am. Chem. Soc.* **2020**, 142, 19110.
- [208] P. Urbankowski, B. Anasori, K. Hantanasirisakul, L. Yang, L. Zhang, B. Haines, S. J. May, S. J. L. Billinge, Y. Gogotsi, *Nanoscale* **2017**, 9, 17722.
- [209] R. Thakur, A. VahidMohammadi, J. Moncada, W. R. Adams, M. Chi, B. Tatarchuk, M. Beidaghi, C. A. Carrero, *Nanoscale* **2019**, 11, 10716.
- [210] M. Seredych, C. E. Shuck, D. Pinto, M. Alhabeb, E. Precetti, G. Deysher, B. Anasori, N. Kurra, Y. Gogotsi, *Chem. Mater.* **2019**, 31, 3324.
- [211] L. Zhang, W. Su, Y. Huang, H. Li, L. Fu, K. Song, X. Huang, J. Yu, C.-T. Lin, *Nanoscale Res. Lett.* **2018**, 13, 343.
- [212] E. B. Deeva, A. Kurlov, P. M. Abdala, D. Lebedev, S. M. Kim, C. P. Gordon, A. Tsoukalou, A. Fedorov, C. R. Müller, *Chem. Mater.* **2019**, 31, 4505.
- [213] J. Peng, X. Chen, W.-J. Ong, X. Zhao, N. Li, *Chem* **2019**, 5, 18.
- [214] Á. Morales-García, F. Calle-Vallejo, F. Illas, *ACS Catal.* **2020**, 10, 13487.
- [215] J. R. B. Gomes, F. Illas, *Catal. Lett.* **2001**, 71, 31.
- [216] J. L. C. Fajín, M. N. D. S. Cordeiro, F. Illas, J. R. B. Gomes, *J. Catal.* **2009**, 268, 131.
- [217] J. L. C. Fajín, F. Illas, J. R. B. Gomes, *J. Chem. Phys.* **2009**, 130, 224702.
- [218] J. R. B. Gomes, J. M. Bofill, F. Illas, *J. Phys. Chem. C* **2008**, 112, 1072.
- [219] J. R. B. Gomes, J. A. N. F. Gomes, F. Illas, *J. Mol. Catal. A: Chem.* **2001**, 170, 187.
- [220] J. R. B. Gomes, J. A. N. F. Gomes, F. Illas, *Surf. Sci.* **1999**, 443, 165.
- [221] J. D. Gouveia, G. Novell-Leruth, P. M. L. S. Reis, F. Viñes, F. Illas, J. R. B. Gomes, *ACS Appl. Bio. Mater.* **2020**, 3, 5913.
- [222] J. D. Gouveia, G. Novell-Leruth, F. Viñes, F. Illas, J. R. B. Gomes, *Appl. Surf. Sci.* **2021**, 544, 148946.
- [223] J. D. Gouveia, Á. Morales-García, F. Viñes, F. Illas, J. R. B. Gomes, *Appl. Catal. B* **2020**, 260, 118191.
- [224] J. D. Gouveia, Á. Morales-García, F. Viñes, J. R. B. Gomes, F. Illas, *ACS Catal.* **2020**, 10, 5049.
- [225] R. Morales-Salvador, J. D. Gouveia, Á. Morales-García, F. Viñes, J. R. B. Gomes, F. Illas, *ACS Catal.* **2021**, 11, 11248.
- [226] I. Persson, J. Halim, H. Lind, T. W. Hansen, J. B. Wagner, L.-Å. Näslund, V. Darakchieva, J. Palisaitis, J. Rosen, P. O. Å. Persson, *Adv. Mater.* **2019**, 31, 1805472.
- [227] J. Zhang, Y. Zhao, X. Guo, C. Chen, C.-L. Dong, R.-S. Liu, C.-P. Han, Y. Li, Y. Gogotsi, G. Wang, *Nat. Catal.* **2018**, 1, 985.
- [228] J. D. Gouveia, J. R. B. Gomes, *Phys. Rev. Mater.* **2022**, 6, 024004.
- [229] J. D. Gouveia, J. R. B. Gomes, *Catal. Today* **2022**, <https://doi.org/10.1016/j.cattod.2022.07.016>.
- [230] J. D. Gouveia, Á. Morales-García, F. Viñes, J. R. B. Gomes, F. Illas, *ACS Nano* **2022**, 16, 12541.



Marta Bordonhos has an M.Sc. in Chemical Engineering (2016, IST, U. Lisboa) and is currently pursuing a Ph.D. in Chemical Engineering at IST. The Ph.D. research is focused on the adsorptive separation of gases in hybrid porous materials in cyclic processes and is being conducted in the Research Centres CERENA and CICECO, under the supervision of Prof. Dr. Moisés Pinto (CERENA, DEQ, IST, U. Lisboa) and the co-supervision of Dr. José R. B. Gomes (CICECO, DQ, U. Aveiro).



**Tiago L. P. Galvão**, holds a Ph.D. in Chemistry, specializing in Physical-Chemistry, from the University of Porto (2013). Since he joined CICECO in 2014, he has combined experimental materials characterization with molecular modeling to unveil nanomaterials' structure, synthesis, and functionality. Currently, he is focused on database production, machine learning, and development of cloud applications for corrosion protection, materials design, and nanosafety. He is the author of more than 30 articles with an h-index of 14.



**José R. B. Gomes** obtained his Degree in Chemistry at the Faculty of Sciences, University of Porto (1995), winning the Prize Teresa da Fonseca for the Best Student, and a Ph.D. in Chemistry, also at the University of Porto (2000). In 2010, he was the recipient of the Vicente de Seabra Medal awarded by the Portuguese Chemical Society. He is a Principal Researcher at CICECO - Aveiro Institute of Materials, where he coordinates the activities in the areas of computer simulation and multiscale modelling. He has an h-index of 42 and co-authored circa 240 scientific articles and 10 book chapters.



**José D. Gouveia** has a Ph.D. in Physics from the University of Aveiro. Since 2019, he has worked as a Researcher at CICECO - Aveiro Institute of Materials, in the Computer Simulation and Multiscale Modelling group. He specializes in the computational modelling of materials at the atomic and electronic levels. Currently, his research focuses on the prediction and understanding of phenomena on the surface of all kinds of materials, mainly with application in the fields of catalysis, green energies, and gas sensing and separation.



**Miguel Jorge** holds a degree in Chemical Engineering from the University of Porto and a Ph.D. from the University of Edinburgh. He has worked as a Researcher in the UK, Portugal, and the USA, and is currently a Senior Lecturer at the University of Strathclyde, in Glasgow. He has authored over 80 scientific publications on development and application of molecular modelling to topics as diverse as adsorption, porous materials design, self-assembly, liquid interfaces, solvation, and partition processes.



**Mirtha A.O. Lourenço** (Ph.D. in Materials Science and Engineering from the University of Aveiro, and Postdoc at Italian Institute of Technology) is currently a Researcher at the Department of Chemistry and CICECO, University of Aveiro. Her research interests include the synthesis and structural elucidation of functionalized porous silicas and carbon-based materials for different adsorption and catalysis applications combining experimental and computational methods. She was recently awarded an ERA-PF HORIZON-WIDERA-2022-TALENTS-02-01 grant to design sustainable porous silicas for optimal CO<sub>2</sub> uptake from biogas.



**José M. Pereira** is a Ph.D. student at CICECO since 2018, under the supervision of Dr. José R. B. Gomes. He participated in the Board of European Students of Technology 2017 Winter Course, in Paris, was awarded a Fulbright scholarship for a 4-month student exchange at Rutgers University, and won the TOP3 award at European Innovation Academy 2021. José's main focus lies on the development of software solutions for scientific applications, with projects such as CarbGen, an online platform for carbon materials design, and ProtoSyn.jl, a novel API for general molecular manipulation and simulation with a focus on protein design.



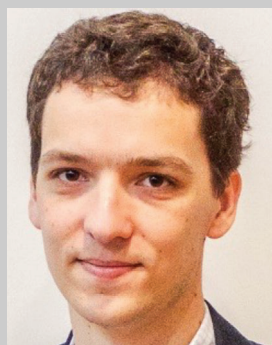
**Germán Pérez-Sánchez** obtained a degree (2006) and a Ph.D. (2010) in Physics from the University of Vigo, with a focus on complete scale theory and critical phenomena of liquids, collaborating with eminent researchers such as Prof. Jan Sengers and Mikhail Anisimov. In 2011, Germán joined Dr. Miguel Jorge's group at the University of Porto, to characterise the synthesis of silica-based mesoporous materials throughout coarse-grained molecular dynamics computer simulations in close collaboration with Dr. José R. B. Gomes at CICECO. Currently, Germán is focused on modelling any class of amphiphilic compounds using coarse-grained MARTINI-based approaches at the University of Aveiro.



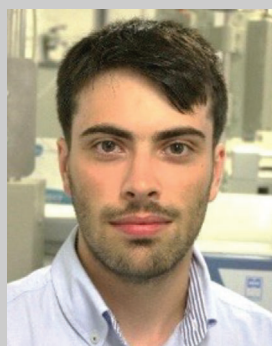
**Moisés Luzia Pinto**, Ph.D. in Physical Chemistry, is an Associate Professor of Chemical Engineering at Instituto Superior Técnico (IST), University of Lisbon. He is currently the Coordinator of research centre CERENA and Assistant Secretary General of the Portuguese Chemical Society. He has been developing research in adsorption materials and related applications over the past 15 years. He is author of 3 international and 1 national patents, 2 book chapters, and ≈92 international papers. He is cofounder of the company Adsorfoam, Scientific Manager of 3 Industrial Research contracts and Scientific Director of 6 Public Research Projects in collaboration with companies.



**Carlos Manuel Silva** is Professor of Chemical Engineering at the University of Aveiro (Portugal) and is a member of CICECO - Aveiro Institute of Materials. His research interests include transport properties (mainly diffusion), separation processes (membranes, ion exchange, adsorption/SMB, SFE), synthesis/characterization of zeotypes for catalysis/separation, modeling, and design. He has an h-index of 40 and co-authored 185 scientific articles, 14 book chapters, more than 200 conferences presentations, and 2 patents.



**João Tedim** is an Assistant Professor at CICECO-Department of Materials and Ceramic Engineering from the University of Aveiro. Awarded with a Ph.D. in Physical Chemistry by the University of Leicester, UK (2009), he has worked for the last 12 years in corrosion protection, namely focusing on the development of materials for controlled release of active species (corrosion inhibitors, biocides, and indicators). He is the author of more than 90 papers, 6 book chapters, and 5 patent applications (h-index 33). In 2017 he received the Carl Wagner Medal Award for Excellence in Research in Applied Electrochemistry and Electrochemical Engineering (EFCE).



**Bruno Zêzere** holds a M.Sc. in Chemical Engineering from the University of Aveiro (2017). He was awarded a Ph.D. grant from the Fundação para a Ciência e a Tecnologia in 2018. Currently, under supervision of Prof. Carlos Silva and Dr. José R. B. Gomes at the Department of Chemistry and CICECO, University of Aveiro, he is pursuing his Ph.D. focusing on the combination of experimental chromatographic techniques, phenomenological modelling, machine learning and classical molecular dynamics computer simulations to determine the diffusivities of bioactive compounds in supercritical fluids and liquids.